2018•2019

Faculteit Industriële ingenieurswetenschappen

master in de industriële wetenschappen: energie

Masterthesis

Lifespan optimization and quantification of bonds on thin-film solar modules

PROMOTOR :

Prof. dr. ir. Michael DAENEN

PROMOTOR :

ing. Jorne CAROLUS

Jasper van Rooy

Scriptie ingediend tot het behalen van de graad van master in de industriële wetenschappen: energie, afstudeerrichting elektrotechniek

Gezamenlijke opleiding UHasselt en KU Leuven

2018•2019

Faculteit Industriële ingenieurswetenschappen

master in de industriële wetenschappen: energie

Masterthesis

Lifespan optimization and quantification of bonds on thin-film solar modules

PROMOTOR :

Prof. dr. ir. Michael DAENEN

PROMOTOR :

ing. Jorne CAROLUS

Jasper van Rooy

Scriptie ingediend tot het behalen van de graad van master in de industriële wetenschappen: energie, afstudeerrichting elektrotechniek

UHASSELT KU LEUVEN

Acknowledgements

This master's thesis describes the research towards lifespan optimization and quantification of bonds on thin-film photovoltaics. It was the final stage of the education to Master of Energy Engineering Technology at Hasselt University and KU Leuven. I am grateful that I was able to complete my master's thesis in EnergyVille 2 where high-quality research is being done into sustainable energy and intelligent energy systems.

The successful completion of this master's thesis would not be possible without several people. First of all, I would like to thank prof. dr. ir. Michaël Daenen for his extensive knowledge and advice. Further, I would like to thank ing. Jorne Carolus for his excellent guidance and support whenever a problem occurred.

Finally, I want to thank my family and friends for the support and motivation that they gave me to successfully complete my entire education.

Table of Contents

List of Tables

List of Figures

List of Abbreviations

ACA	Anisotropically Conductive Adhesives
CIGS	Copper Indium Gallium Selenide
DH	Damp-heat
ECA	Electrically Conductive Adhesives
ECT	Electrically Conductive Tapes
EDX	Energy Dispersive X-ray
ICA	Isotropically Conductive Adhesives
PV	Photovoltaic
R_c	Contact resistance
SEM	Scanning Electron Microscope
TC	Thermal Cycling
TFPV	Thin-film photovoltaic
TLM	Transmission Line Model
USS	Ultrasonic soldering
USW	Ultrasonic welding

Abstract

The research group Energy Systems Engineering (ESE) is part of imo-imomec, an affiliated lab of imec. ESE examines the reliability and efficiency of photovoltaic systems. One focus point of the research group is the integration of thin-film photovoltaics (TPFV) in building-integrated photovoltaics. The aim of this master's thesis is to optimize the lifespan and efficiency of the connection between molybdenum back contacted CIGS TFPV and the conductor to the junction box.

To optimize the connection, three methods are compared: ultrasonic soldering (USS), ultrasonic welding (USW) and electrically conductive tapes (ECT). The connections were subjected to accelerated stress tests: damp heat (DH) and thermal cycling (TC) tests based on the IEC 61646 norm. While doing these tests, the electrical contact resistance is characterized on fixed intervals. Next, scanning electron microscope (SEM) images are made of pristine samples as well as stressed samples to do a visual inspection of the degradation.

The first measurements show that the resistance of the ECT was about 1000 times higher than USW and USS. TC did not cause degradation of the samples. Meanwhile, DH tests did cause degradation. After 300 hours multiple ribbons, which were attached with USS, started to detach and the contact resistance increased. The contact resistance of USW bonds increased after 440 hours but the ribbons did not detach from the substrate. The conclusion is that USW is the best method to create bonds on molybdenum back contacted CIGS TFPV.

Samenvatting

Energy Systems Engineering (ESE) is een onderzoeksgroep die deel uitmaakt van imo-imomec, een geaffilieerd labo van imec. ESE onderzoekt en optimaliseert de betrouwbaarheid en efficiëntie van PV-systemen. Eén van de focuspunten is de integratie van dunnefilmzonnecellen (TFPV) in gebouwgeïntegreerde zonnemodules. Het doel van deze masterproef is de levensduur en efficiëntie van de verbinding tussen CIGS TFPV met molybdeen achtercontactlaag en de elektrische geleider te optimaliseren.

Om deze verbinding te optimaliseren werden drie verbindingsmethodes getest: ultrasoon solderen (USS), ultrasoon bonden (USW) en elektrisch geleidende tapes (ECT). De verbindingen zijn onderworpen aan geaccelereerde stresstesten: dampheat- (DH) en thermalcycling- (TC) testen gebaseerd op IEC 61646. Tijdens de testen werden de verbindingen gekarakteriseerd door de elektrische contactweerstand te meten op vaste intervallen. Daarna werden met behulp van de scanning electron microscope beelden gemaakt van samples voor en na de stresstesten om een visuele inspectie te doen van de degradatie van de verbindingen.

De eerste metingen gaven weer dat de weerstanden van ECT ongeveer 1000 maal hoger lagen dan USS en USW. De verbindingen degradeerde niet door TC. Daarentegen lieten meerdere USS-verbindingen na 300 uur DH-testen los en steeg de contactweerstand. De contactweerstand van USW verbindingen steeg na 440 uur zonder loslatende verbindingen. De conclusie is dat USW de beste methode is om verbindingen te maken op CIGS TFPV met molybdeen achtercontactlaag.

1 Introduction

The research group Energy Systems Engineering (ESE), led by prof. dr. ir. Michaël Daenen, is part of imo-imomec, an affiliated lab of imec. The research group is located at the research lab of EnergyVille2, Genk. Besides Hasselt University and imec also KU Leuven and VITO uses the lab to do research on sustainable energy and intelligent energy systems.

ESE examines the reliability of photovoltaic (PV) systems. One of focal points of the research group is the research into thin-film solar (TFPV) modules, these are interesting for building-integrated photovoltaics (BIPV).

TFPV solar cells are made of several functional layers. TFPV research is still ongoing what results in multiple variations in stack sequence and used materials. This master's thesis uses TFPV solar cells with copper indium gallium diselenide (CIGS) as absorber material with a stack sequence as shown in Figure 1. The function of each layer in TFPV solar cells are explained in the next paragraph.

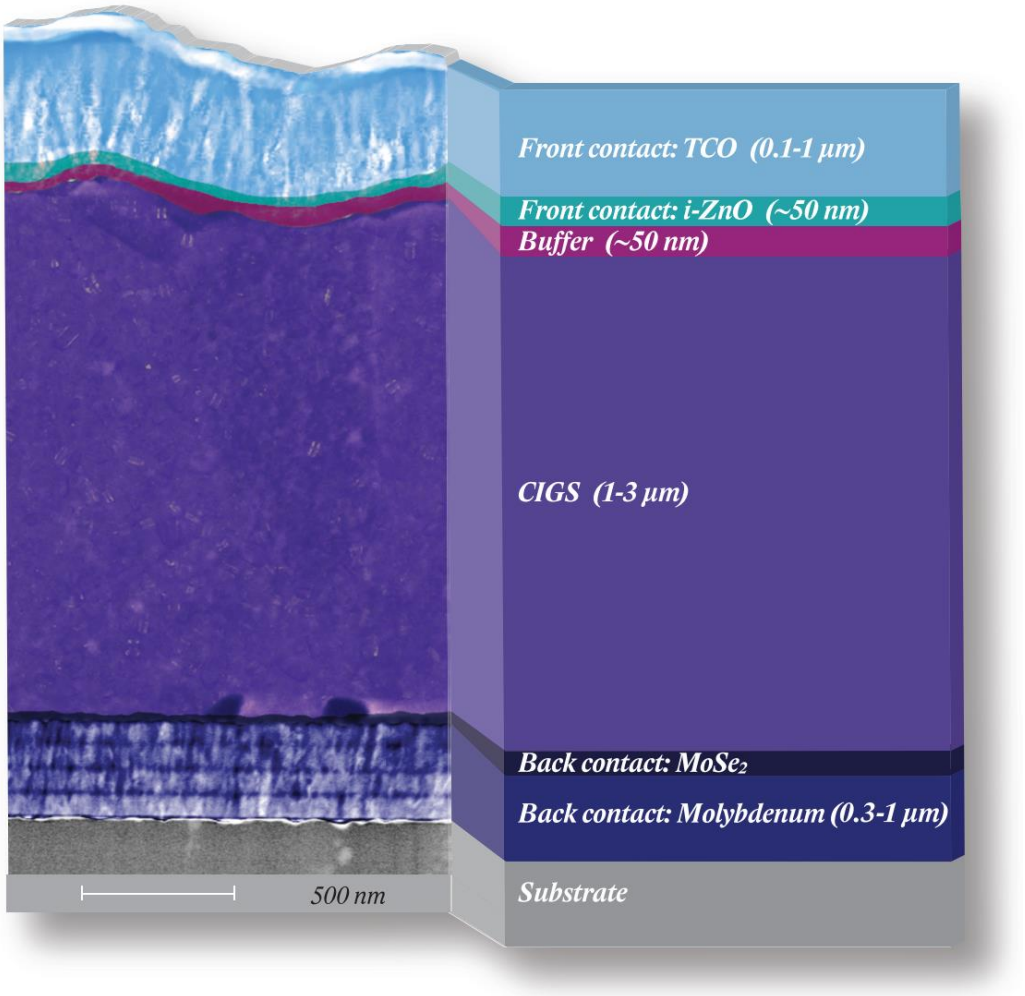

Figure 1: Overview of the typical layers in CIGS solar cells [1, p. 12]

The bottom layer, named the substrate, is made of soda lime glass. This layer provides stability for the whole solar cell. On top of the substrate is the back contact layer, necessary to transport the generated holes from the absorber layer. The back contact is made of molybdenum which has good conductivity and adhesive properties.

Between the molybdenum back contact layer and the absorber layer is a small layer of molybdenum diselenide ($MoSe_2$). This layer grows when the absorber layer is deposited, as a result an unwanted resistance is created.
Next, is the absorber layer. This is a p-type polycrystalline semiconductor made of $Cu(In,Ga)Se_2$ (CIGS) which has a high optical absorption coefficient. This is needed because this layer absorbs the light and generates the electron-hole pairs. To create a heterojunction, a n-type buffer layer made of CdS is added.
On top of the buffer layer is a highly resistive front contact layer to avoid shunt paths in the solar cells. Finally, an aluminium-doped ZnO layer is placed on top. The incident light passes through this top layer into the absorber layer and is the second contact layer that conducts electrons [1].

1.1 Problem statement

Since the combination of TFPV with BIPV is still in research phase, there are still some reliability problems. One of these reliability problems is the lifespan of the connection between the solar cells and the conductor to the junction box. In order to allow the electrically generated current to flow from the solar cell to the junction box, an aluminium conductor is used.

Another problem is the efficiency of the bonds between solar cell and conductor. In other industries and applications such as aerospace, automotive and electronics, there already has been done research to various connection methods and optimal bonding parameters [2]–[5]. Three of these connection methods that can be used, but which are not optimised yet for TFPV are:

- ultrasonic welding,
- ultrasonic soldering,
- electrically conductive adhesives.

A first method is ultrasonic welding. This bonding method connects conductor and solar cell under external pressure with the use of ultrasonic vibrations. There is no extra additive material used for the connection.

Ultrasonic soldering is a second method that will be used to connect the aluminium conductor to the solar cell. In contrast with ultrasonic welding, an additive material to create the connection is used. Ultrasonic vibrations replace the function of the chemical flux in classic soldering applications.

A last way to create the bonds is with the use of electrically conductive adhesives. This electrical conductive material is used as tape or glue.

1.2 Objectives

The main goal of this master thesis is to find the most efficient and reliable solution to maximize the lifespan of the electrical connections on TFPV modules. Besides that, the losses due to contact resistance between TFPV and conductor should be minimized. To achieve this, the main objective can be divided into several sub-objectives.

A first objective is to do a literature study. The following topics will be studied:

- connection methods;
- methods to accelerate the degradation of the connections;
- methods to quantify the efficiency of the connections.

A second objective is to make an accelerated degradation method. Contemporary solar panels have an expected lifespan of between 20 and 25 years. To do the research project in several months, it is necessary to accelerate the degradation of the connections.

Creating a testing method to quantify the degradation of the connections is a third goal. On the one hand, the search is for the connection with the lowest contact resistance, on the other hand must the lifespan of the connection be maximized. Measuring equipment from the EnergyVille2 laboratory can be used for this. With the help of these tests the initial and final state of the connections can then be compared. In addition, the different connection methods are compared.

The fourth objective is to determine the optimal parameters with which the connections are made. With ultrasonic bonding and soldering, there are several variable parameters that influence the quality of the connection. For ultrasonic welding it is important to investigate the influence of bonding energy, pressure and amplitude. With ultrasonic soldering, the soldering temperature and the ultrasonic power are important.

The last objective is to document the four objectives above in a report. This report therefore contains the literature study, the methods used to degrade the connections on the solar modules and to test them on both electrical and mechanical level. Finally, the results of the tests including the optimal production parameters for the electrically conductive adhesives and the ultrasonic bonding and soldering will be described.

1.3 Methodology

Using the literature study, existing applications of conductive adhesives, ultrasonic welding and soldering will be studied. Next to the connection methods, existing characterisation and accelerated degradation methods will be studied. With the use of the found information a test case will be made to examine and accelerate the degradation of the connections between solar cell and conductor.

The next step is the creation of the samples. The first group of samples will be made on pure molybdenum. Parameters of each connection method can easily be tested because bonds can directly be made on this substrate. The second group of samples will be made on substrates with a CIGS layer on top of the molybdenum as shown in Figure 1. Before bonds can be created on the molybdenum back contact layer, the upper layers must be removed. With the use of a scraping tool the upper layers are removed from the molybdenum. The difficulty hereby is to also remove the $MoSe_2$ layer because the efficiency drops because of the ohmic resistance. Both sample groups can then be compared to determine the influence of $MoSe_2$ on the efficiency.

The third step is to set up the method to measure the degradation characteristics of the connections. To quantify the degradation, the electrical resistance will be measured, and an image will be made with a scanning electron microscope (SEM). Afterwards, the samples will be stressed to degrade. The samples will be tested again afterwards. The received data will be analysed to determine the degradation.

Together with the characterization, the accelerated degradation will start. After measuring a reference (no degradation), the samples will be stressed to accelerate the degradation process. This will be done via two methods. The first one is thermal cycling whereby the samples will be heated and cooled down between -40 °C and 85 °C for 200 cycles (TC200). Damp-heat testing is a second method. The samples will be exposed for 1000 h to a climate with temperature of 85 °C and a relative humidity of 85% (DH1000).

Furthermore, it is also important to document the parameters in which the various connections are realized. It must be possible to reproduce the connections in the samples.

Finally, the results must be processed. Only a limited number of test samples can be tested. The expectation is that the degradation process will take several weeks. It is therefore important to determine in advance with which parameters the test samples will be made. Afterwards, the test samples are analysed to determine the optimal process parameters in order to maximize the life of the TFPV panels. The results are documented in the written part of this master's thesis.

1.4 Outline of the dissertation

In Chapter 2, the literature review is discussed. First, the structure of TFPV will be discussed in Section 2.1. Next, the bonding techniques will be explained in Section 2.2. A third topic that will be discussed are the methods to accelerate the degradation of the samples. Lastly, in Section 2.4 the different measuring methods are discussed.

In Chapter 3, the used materials and methods to compare the bonding techniques are explained. First, the explanation of the sample matrix is given. Secondly, the used substrate materials to create the bonds on and the preparation of the substrates is discussed. Next, the techniques to realise the bonds and the setups of the degradation and characterization methods are explained in detail. This will include the used equipment and parameters.

In Chapter 4, the results of the characterization measurements will be discussed. The results will be described and discussed per bonding method. Further, SEM images and optical images will be studied and compared from before and after the stress tests. Lastly, an overview is given which summarizes the results and compares them.

In Chapter 5, the conclusions are presented.

2 Literature review

The literature study consists of four main topics as shown in Figure 2. Section 2.1 focuses on the structure of thin-film photovoltaics and the used materials. Section 2.2 reviews the working principle and the operation parameters of each connection method. Next, in Section 0 the different methods to stress the joints are explained according to international standards. Finally, Section 2.4 discusses the possible methods to characterize the connections of TFPVs.

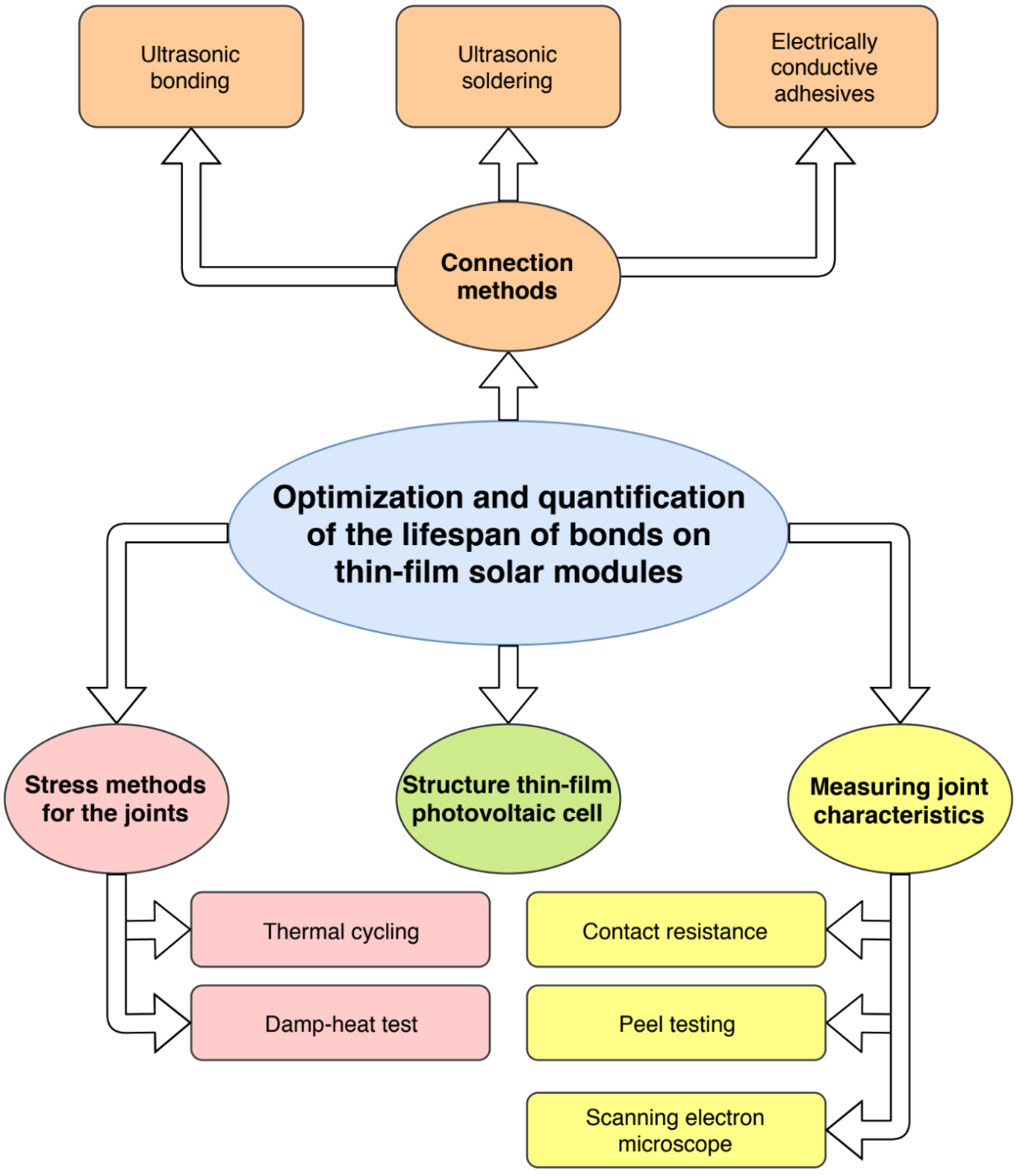

Figure 2: Overview of the reviewed literature topics

2.1 Structure thin-film photovoltaic cell

This chapter is based on [6], the different structures of thin-film photovoltaic (TFPV) and used absorber materials will be explained in this paragraph.

The structure of TFPV contains four basic layers as shown in Figure 3. The stack sequence of three layers is always the same. However, the layer to keep mechanical and thermal stability can be the top layer or the bottom layer, respectively called the superstrate and substrate. A difference between the superstrate and substrate is that the superstrate needs to be as transparent as possible to let the light through. On the other hand, the substrate can be opaque because it only provides mechanical and thermal stability.

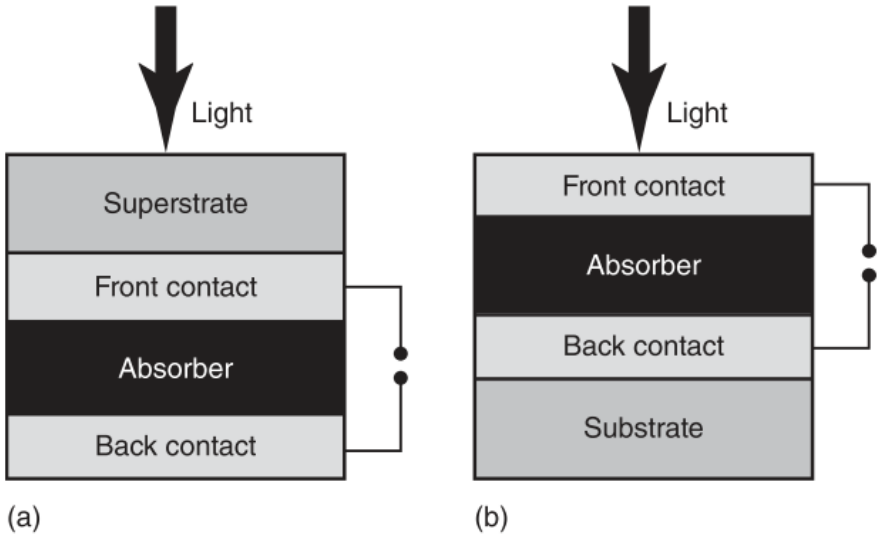

Figure 3: Superstrate configuration (a) and substrate configuration (b) [6, p. 20]

The other three layers are the front contact, the absorber and the back contact. The front and back contact layers are the electrical connections that conducts the electrical energy towards the conductors. To maximize the efficiency the front layer has an antireflection coating and the back contact layer will reflect the appearing light.

The last layer in a TFPV is the absorber. This layer is in between the front and back contact. The absorber converts the incoming light into electrical energy. To maximize the converting process efficiency the absorptance factor needs to rise to maximum as fast as possible after exceeding the band gap. Further, a high mobility and low recombination rates and high open-circuit voltages results in a more efficient absorber layer [6].

2.1.1 Cu(In,Ga)Se2

Copper Indium Gallium Selenide (CIGS) solar cells are made with an absorber material consisting of $Cu(In,Ga)Se_2$. These types of solar cells are made according to the substrate configuration as shown in Figure 4. The substrate is made of soda-lime glass. To create a back contact, a Molybdenum layer with a thickness of 1 µm is sputtered on the substrate. Next, the $Cu(In,Ga)Se_2$ layer (varying between 1 – 2 µm) is added on the Mo layer. Before adding this layer, the CIGS layer is grown. This can be done with various techniques, the most used and efficient techniques are co-evaporation and sputtering [7]. Next, the CdS layer with a thickness of 50 nm is added via chemical bath deposition. Next, an undoped i-ZnO

layer (typically 50 – 70 nm) is sputtered, followed by a heavily doped ZnO:Al window layer to complete the hetero junction [6].

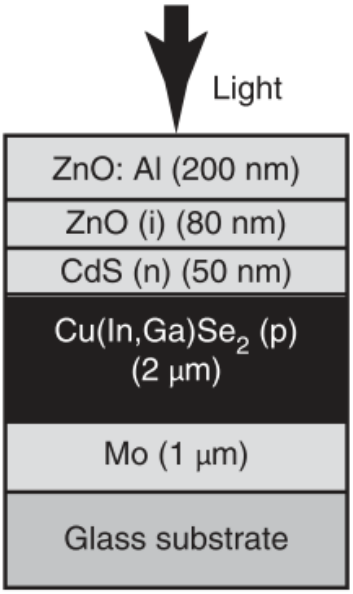

Figure 4: CIGS solar cell structure [6, p. 22]

2.2 Connection methods

This chapter contains the three different connection methods that will be examined in this thesis on reliability and lifespan. Ultrasonic welding and ultrasonic soldering are methods that attaches a metal ribbon on the TFPV. The ribbon conducts the generated electrical current to the junction box. The last method, electrically conductive adhesives (ECAs), is a conducting tape. This tape is made with two materials: a glue to stick the ECA and a conducting material [8]. In this chapter the working principle of each method and the corresponding influence of each process variable is explained.

2.2.1 Ultrasonic welding

Ultrasonic welding is a technique that uses ultrasonic vibrations under an external pressure to connect two materials to each other. This can be two similar metals but it is also possible to join two various metals or weld a metal piece to a metallized substrate such as ceramics or glass [9].

An ultrasonic welding machine has three elementary parts as shown in Figure 5. These are:

- The electrical part that generates an electrical sine wave signal. The signal is the input for the amplifier that will supply the transducer.
- The electromechanical transducer converts the electrical power into mechanical vibrations.
- The mechanical part consists of the welding tool and anvil. The welding tool is connected to the electromechanical transducer via the horn. The anvil is used with the welding tool to clamp the work pieces [9].

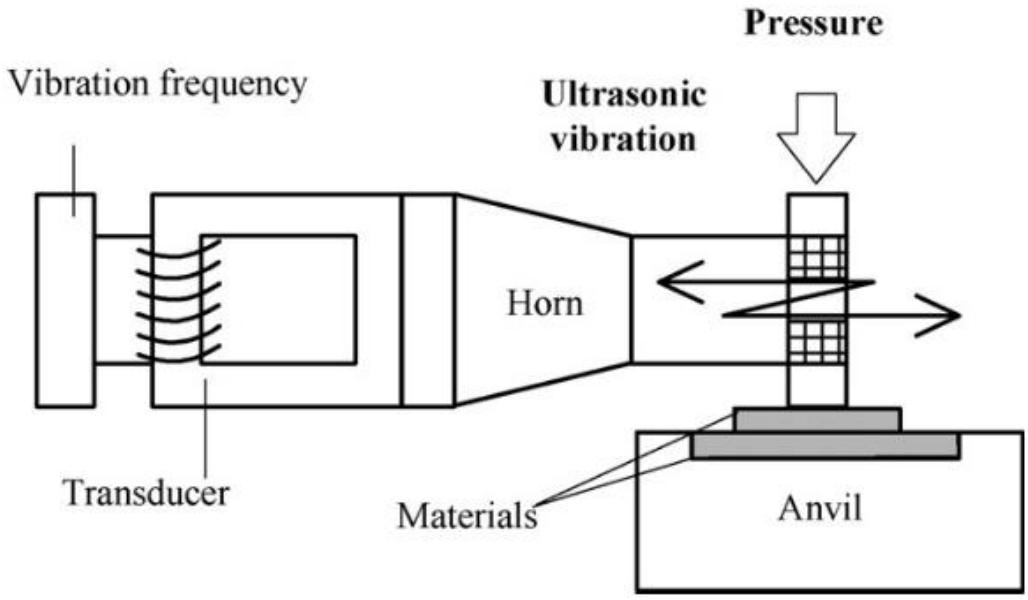

Figure 5: Basic principle of ultrasonic welding [10, p. 955]

There are five main process parameters to create a bond. The value of each parameter depends on the kind of materials used and the thickness of the material contacting the welding tip [9]. These parameters are:

- frequency, varies between 15 – 75 kHz depending on the used equipment;
- vibration amplitude, generated amplitude varies between 30 – 60 μm;
- clamping force; the force used to clamp the materials varies between 2 - 5 bar;
- power,
- welding time,
- energy [11, p. 264].

2.2.2 Ultrasonic soldering

The second method that will be tested to create bonds on the solar cells is ultrasonic soldering. In classic soldering applications a chemical flux is used. By ultrasonic soldering this chemical flux is replaced by mechanical energy in the form of ultrasonic vibrations [12].

The ultrasonic soldering process is described by [13], [14] using a schematic overview as seen in Figure 6. First the solder is heated by the tooltip. This molten solder is applied to the substrate. The molten solder can now transfer the ultrasonic vibrations coming from the tooltip. When the tooltip sends high-frequency vibrations, this will cause cavitation in the solder. The energy from the bursting cavitation bubbles is used to remove the oxide layer from the base material. Now the liquid solder can wet and bond to the base material.

Beside the removal of the oxide layer, the ultrasonic energy from the tooltip forces the solder into crevices and micropores in the substrate. A last effect caused by the ultrasonic vibrations is that the gas bubbles are pressed out. These side effects provide a larger contact surface, resulting in a better bond quality.

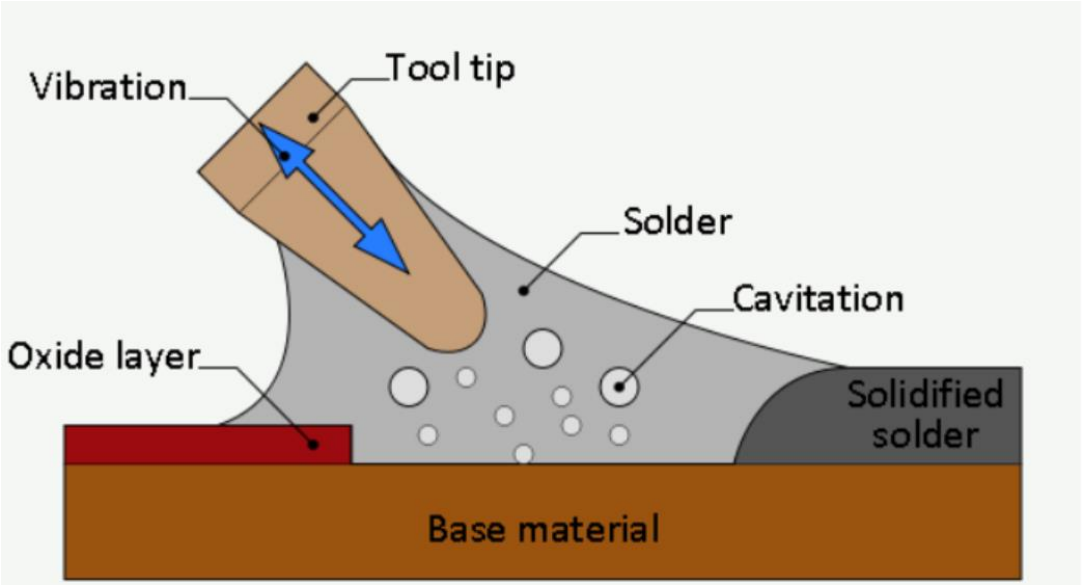

Figure 6: Ultrasonic soldering working principle [14]

The quality of the connection depends on a few parameters. These has been discussed by [15]. Depending on the used tool some will be fixed, when using a fully automatic machine, or will vary because the use of a manual ultrasonic solder.

The temperature and ultrasonic power are two parameters that can be set at a fixed value independent of the machine used. The temperature needs at least be higher than the liquidus temperature. Next to that research shows that increasing the temperature will improve the tensile strength. On a certain temperature the tensile strength will remain constant, this depends on the material of the solder used. The ultrasonic power also can be set on the ultrasonic soldering tool. This power varies depending on the vibration amplitude and the frequency. The ultrasonic vibration can be activated with a foot pedal when using a manual tool.

In addition to the temperature and the ultrasonic power, the quality of the joint may vary depending the soldering time and the applied pressure. When using a fully automatic ultrasonic soldering machine these parameters can be set at a fixed value. In contrast to a manual ultrasonic soldering tool, the soldering time and applied pressure is controlled manually by the operator.

2.2.3 Electrically conductive adhesives

The last method to conduct the current is using electrical conductive adhesives (ECA). ECA replaces tin-lead solders in the semiconductor industry. There are different reasons to use ECA instead of the standard solder techniques, such advantages are the limited environmental impact (no use of lead) and the lower heat addition allowing the use of heat sensitive components. The advantages, structure and different types of ECA have been discussed by [16]. The relevant topics for this master's thesis will be pointed out in this chapter.

In contrast to ultrasonic soldering and bonding applications, there are two essential materials for ECA. On the one hand there is an electrical conductive material to provide the electrical properties also known as the filler. On the other hand, there is an organic/polymeric material to provide the physical and mechanical properties.

ECA can be divided in two categories based on filler loading level. A first category is the anisotropically conductive adhesives (ACA). These adhesives have 3 – 5 µm sized conductive fillers. The other category is called the isotropically conductive adhesives (ICA). The ICAs have fillers with a size between 1 – 10 µm.

A result of the difference of the fillers is the conducting directions. ICA conduct current in all x-, y- and z-directions. Whilst ACA only conducts in the z-direction. This inequality is based on the percolation theory. This is a simple probabilistic model with the following question: "What is the probability that there exists an open path, i.e., a path all of whose edges are open, from the origins to the exterior of the square $S_n := [-n, n]^2$?" [17, p. 572].

Using this percolation theory with ECA, this is converted to the volume, shape and size of the fillers. At a certain point the conductivity will rise abruptly as seen in Figure 7, this is called the perculation threshold. Figure 8 shows this difference in a schematic overview. The volume density by ACA is below the perculation threshold. Meanwhile, ICA have a higher density so that they are above the perculation threshold resulting in a higher conductivity. This difference in filler concentration explains why ACA only conducts in the vertical direction and ICA conducts in every direction.

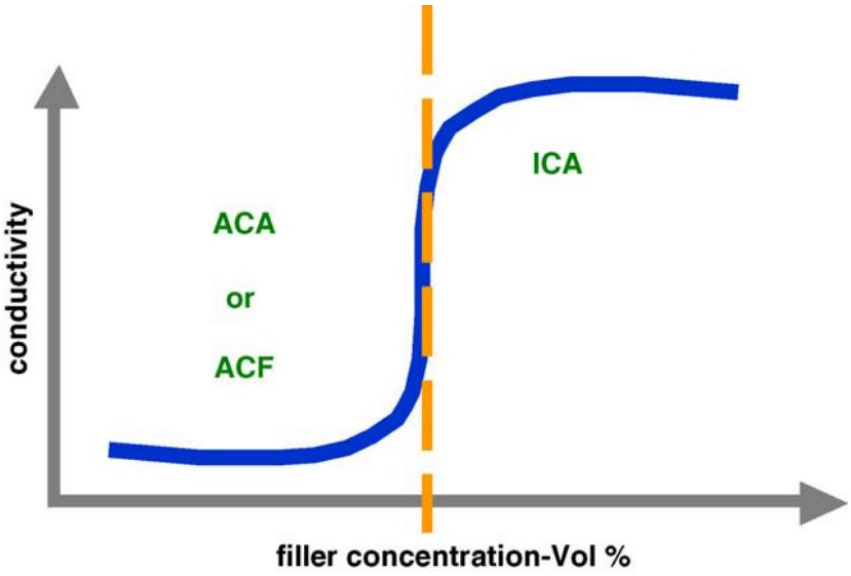

Figure 7: The conductivity rises strongly at the perculation treshold [16, p. 4]

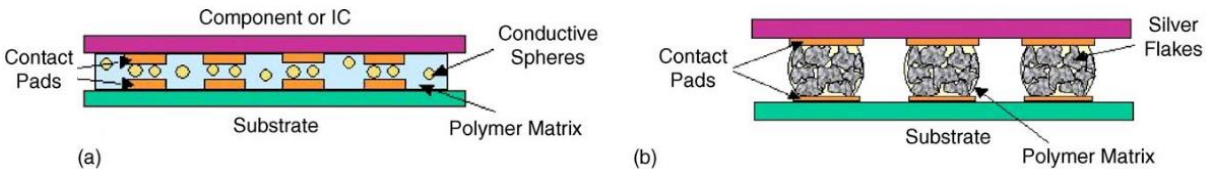

Figure 8: Schematic illustrations of (a) ACA and (b) ICA [16, p. 4]

2.3 Stress methods for the joints

One of the objectives of this master's thesis is to investigate the best bonding method to maximize the lifespan of TFPV. Since the expected lifetime is over 20 years, there are standardised test methods to accelerate degradation. These are included in IEC 61215 and IEC 61646. This are two standards that describes performance and stress tests for respectively crystalline silicon and thin film photovoltaic modules. These test have been explained by [18].

2.3.1 Thermal cycling

A first way to stress the TFPV modules is thermal cycling (TC). Changing the temperature stresses the joints because of the different thermal expansion coefficients of the used materials. This cycle is repeated 200 (TC200) times following the temperature profile shown in Figure 9.

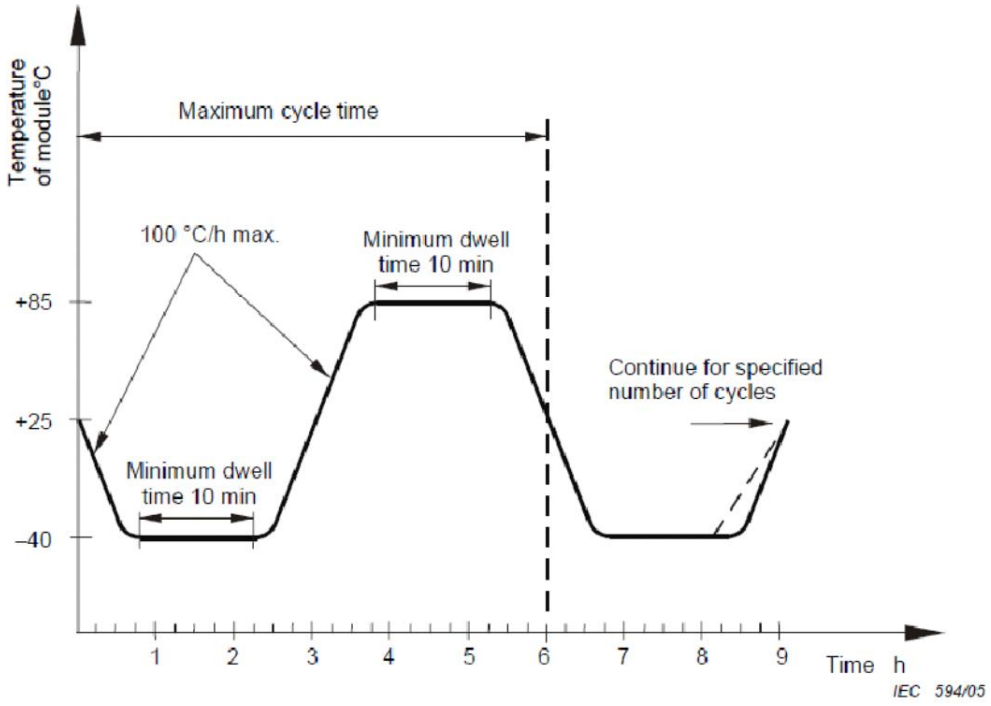

Figure 9: Temperature profile for thermal cycling [18, p. 10]

The cycle varies the temperature between -40 °C ± 2 °C and +85 °C ± 2 °C. Each cycle, the minimum as well as the maximum temperature needs to be maintained for at least 10 minutes. Raising and lowering the temperature must be done with a maximum of 100 °C per hour.

2.3.2 Damp-heat test

The damp-heat (DH) test is exposing the TFPV module for 1000 hours (DH1000) to an environment with a temperature of 85 °C ± 2 °C and a relative humidity of 85% ± 5%.

Normally, this method is used to stress the lamination process and the edge sealing from humidity. After this test, delaminations and cell corrosion will be visible. Even if the solar module did not fail to this test, it has been stressed so it becomes fragile for mechanical characterization tests. No encapsulated samples are used in this master's thesis, so damp heat stressing will immediately affect the interconnections.

2.4 Measuring joint characteristics

The main objective of this master's thesis is to examine the degradation of the three different bonding methods. There are various ways to check the degradation. These comparison methods can be divided into three categories: electrical, mechanical and visual comparison. This chapter will discuss a method for each category to measure the degradation.

2.4.1 Contact resistance

Characterising the electrical degradation of the connections can be done via measuring the contact resistance before and after stress testing. The variation in contact resistance is a way to determine the degradation and to compare the three bonding methods. The contact resistance should be as low as possible to maximize the efficiency.

Measuring the contact resistance can be done via the transmission line model (TLM) [19]. With this model three to five fingers are parallel to each other as shown in Figure 10. Via measuring the current I and voltage-drop V, the total resistance between two contacts can be calculated.

$$R = \frac{U}{I}$$

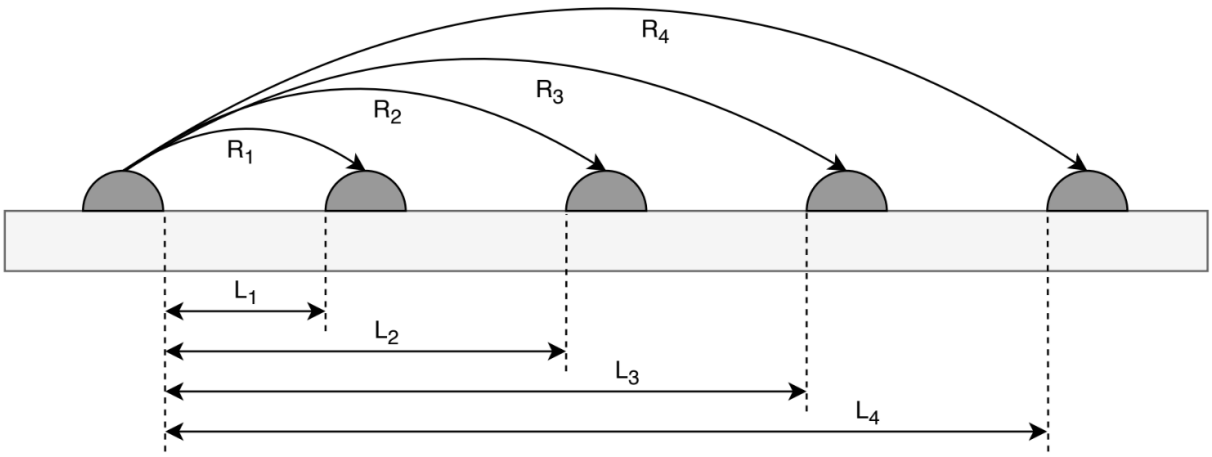

Figure 10: Measurements to determine contact resistance. Figure based on [20, p. 2]

To determine the contact resistance R_C, all the calculated resistances must be plotted in function with the corresponding length as shown in Figure 11. The next step is extrapolating the linear function towards the point where the length is zero. The remaining resistance is the double value of the contact resistance.

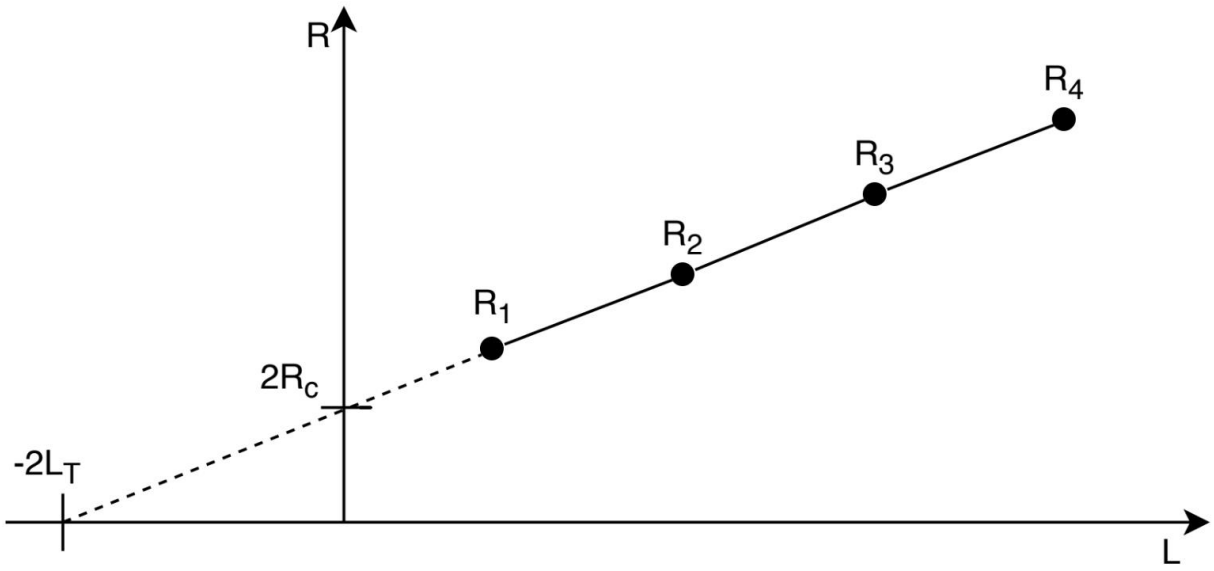

Figure 11: Contact resistance determination using TLM

To make a correct comparison between the bonding methods, the specific contact resistances or contact resistivity (ρ_c) must be compared. This is the resistance per surface area. The contact resistivity can be calculated with:

$$\rho_c = R_C * L_T * W$$

R_c is the contact resistance, L_T is the transfer length and W the finger length [20].

2.4.2 Peel testing

Peel testing is used to measure the mechanical strength of bonds. The force used to separate two materials is directly usable as measure of the bond strength. The peel method to measure the bond strength varies depending on the used materials. These peel tests have been summarised by [21].

A schematic overview of the different peel test methods is given in Figure 12. The first one is called the fixed arm peel test. This test method peels a flexible material of a rigid substrate with a constant angle. The peeling angle can vary between 45° and 180°. To maintain a constant peeling angle, the substrate or the fixed arm must move with a constant speed while peeling the flexible material off.

A second peeling method, T-peel test, is often used to test the peeling strength between two flexible materials. The peeling angle is in most cases 180°. In contrast to the fixed arm method, the bonded part will not be guided.

Wedge and floating roller peel tests are used for rigid-to-rigid bonds. The wedge peel test presses a wedge between the two materials. The floating roller method uses two rollers with a fixed distance from each other which guides the peel arm. The other arm is guided over the rollers with a constant speed.

A fifth method is the climbing drum method. Hereby is the peel arm attached to a drum. To split the bond, a torque is generated to rotate the drum. This torque includes also the energy necessary to bend the peel arm strip. To determine the bond strength, an unbonded strip

with the same specifications needs to be wound up. The difference between the torque with bonded strip and unbonded strip is the bond strength.

The last method to measure the bond strength is the mandrel peel test. This method uses a mandrel to bend the flexible peel arm around. To peel off the flexible specimen a force is applied on the flexible peel arm. To prevent fractures in the flexible peel arm, the curve angle around the mandrel can be controlled [22].

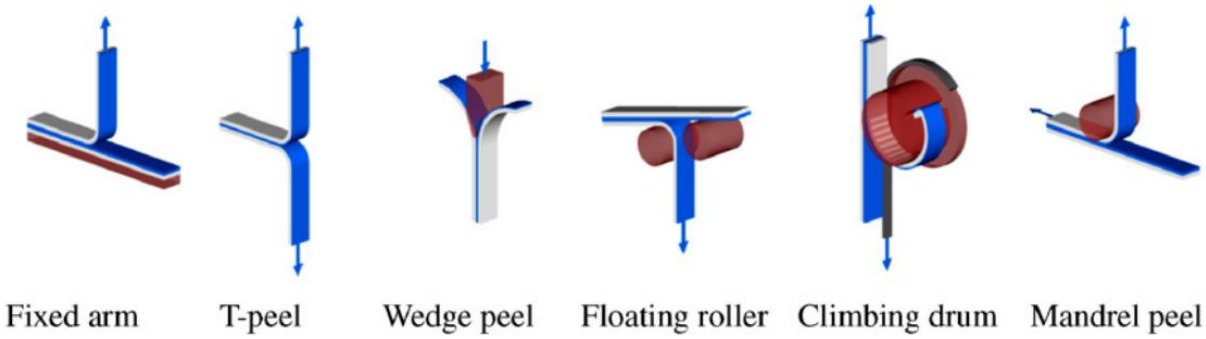

Figure 12: Schematic overview of various peel tests [21, p. 154]

2.4.3 Scanning electron microscope

The scanning electron microscope (SEM) is used to make images of specimen with a maximum resolution better than 1 nm. Using the SEM, it will be possible to visualize cracks after stressing the samples. These samples can then be compared with the image samples from before the stress tests.

The working principle of the SEM is described by [23]. The basic principle is as follows: an electronic beam (primary electrons) scans the surface of interest. The electrons that strike the surface, cause various generated signals. These are shown in Figure 13. The transmitted signals are collected with a detector. Then, the collected signals are used to create an image.

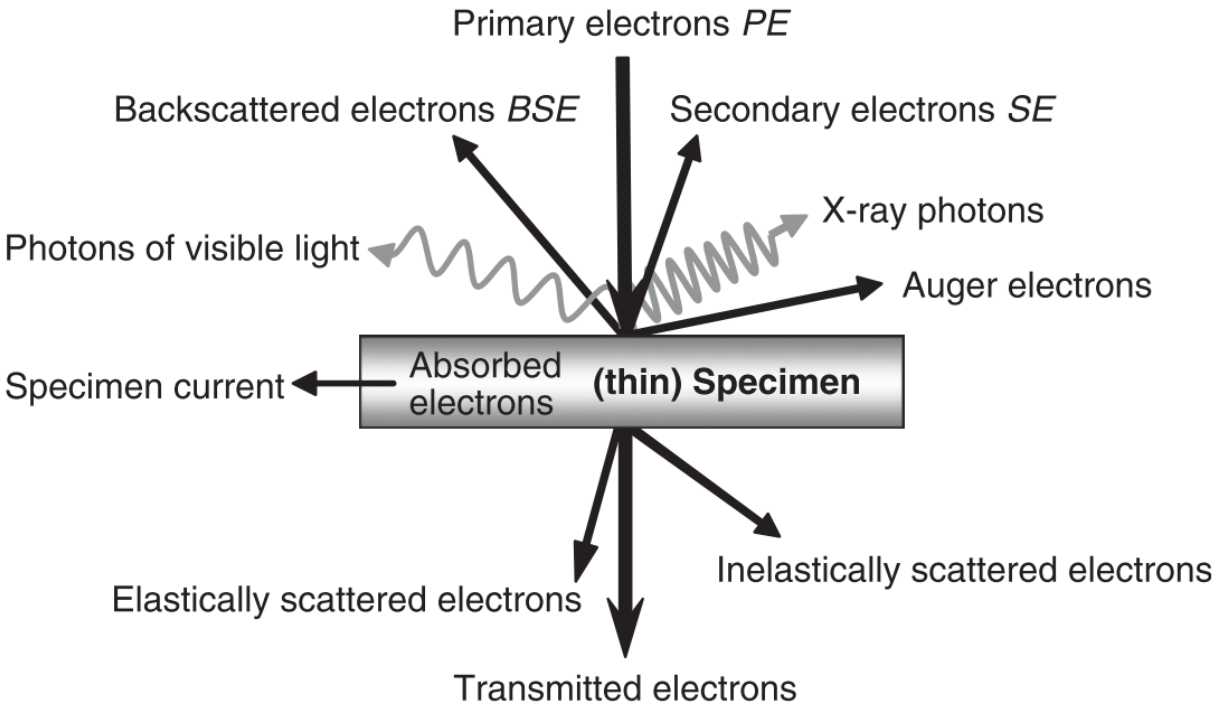

Figure 13: The resulting signals when a primary electron hits the specimen [23, p. 20]

The incoming electron beam consists of primary electrons. The backscattered and secondary electrons are used to create the image. The variation of the electron signal intensity that is detected, will create the contrast in the image. The electron signal intensity depends on chemical composition and surface topography.

Besides the backscattered and secondary electrons, there are other signals generated because of the incoming primary electrons. These are Auger electrons, X-ray photons and photons of visible light. If the specimen thickness is around a few hundred nanometres, there will be transmitted electrons through the specimen.

The smallest difference that can be detected is mainly based on the wavelength λ of the probing radiation. A smaller wavelength results in a smaller difference that can be seen.

Figure 14 shows the basic components of a SEM. [23] describes these as follows:
"- an electron source;
- lenses and apertures;
- coils for scanning the beam;
- control electronics and high-voltages supplies;
- a deflector/acquisition system for collecting and processing the signal information;
- a monitor to display the information;
- a vacuum system for the source, column and specimen chamber."

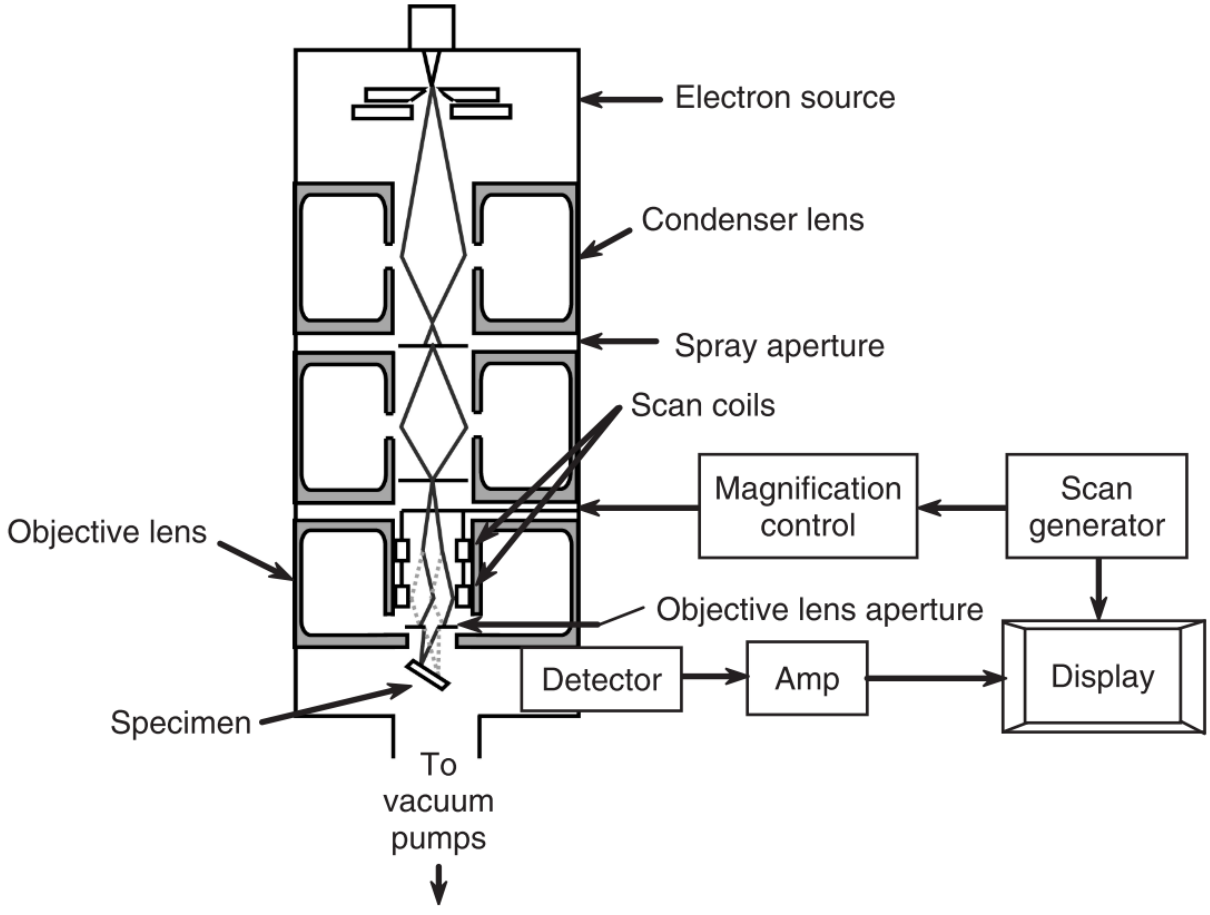

Figure 14: Simplified schematic diagram of the basic components of a SEM [23, p. 20]

Applying a high voltage (range 30 kV – 100 kV) to an electron gun results in a beam of electrons. The released electrons are then focused towards the specimen with

electromagnetic lenses. Next to the wavelength, also the deviations in electromagnetic lenses determine the resolution. These deviations focus the electrons slightly different, as a result the beam has a disc of least confusion. This disc has a finite minimum diameter instead of infinitely sharp point.

When the primary electrons strike the sample, it can be deflected so called backscattered electrons. Another possibility is that the electron goes through the specimen in case of thin samples, then they are called transmitted electrons.

Scanning with an electron microscope damages the specimen. First the electronic beam that strikes the sample is a form of damage. Next to that, bad electrical conductors will charge the bulk of the specimen negatively what will affect the image.

3 Materials and methods

3.1 Sample matrix

To get an overview of the necessary samples that will be compared, a sample matrix is made. This matrix is shown in Table 1. A first difference is based on substrate material, the first group has pure molybdenum (Mo) as base layer while the second group has molybdenum diselenide ($MoSe_2$) as base layer.

Next, each material group is divided based on bonding type. These are ultrasonic welding (USW), ultrasonic soldering (USS) and two electrical conductive tapes. The bonds made on the pure molybdenum samples are only used to determine the contact resistance. With these measurements, a comparison can made with the bonds made on $MoSe_2$.

The $MoSe_2$ samples are exposed to two different stress tests. These are thermal cycling and damp heat. The exact parameters of these tests are explained in 3.4. While performing these tests the samples are measured once per day to characterize the degradation.

Lastly there are two extra samples made for each bonding type. These samples can be used to make images with the SEM if there is delamination in the stressed samples.

Table 1: Samplematrix

Type	Bonding type	Use	#
Mo	USW	R_c-characterization	5
	USS	R_c-characterization	5
	1181-tape	R_c-characterization	5
	T12456-tape	R_c-characterization	5
MoSe2	USW	Thermal cycling with R_c-characterization	5
		Damp-Heat with R_c-characterization	5
		Scanning electron microscope	2
	USS	Thermal cycling with R_c-characterization	5
		Damp-Heat with R_c-characterization	5
		Scanning electron microscope	2
	1181-tape	Thermal cycling with R_c-characterization	5
		Damp-Heat with R_c-characterization	5
		Scanning electron microscope	2
	T12456-tape	Thermal cycling with R_c-characterization	5
		Damp-Heat with R_c-characterization	5
		Scanning electron microscope	2

3.2 Substrate materials and sample preparation

As stated in 3.1 there are two different substrates used. The first substrate is pure molybdenum. These are cleaned with wipes which contain isopropyl alcohol (IPA). There are no other steps needed to create bonds on the substrate.

The second group of substrates that are used to create samples require more preparation. The substrates are delivered with a CIGS layer on top of the Molybdenum layer. The CIGS layer first needs to be removed with a mechanical scraping tool. After the removal of the CIGS layer, there is a $MoSe_2$ layer which causes an extra unwanted resistance between the ribbon and back contact layer. This layer cannot be removed with a scraping tool.

All the substrates have the same size. The size of the samples is 50 x 50 mm and each sample has five ribbons attached to it whereby the centre-to-centre distance is 10 mm. The distance in between can vary depending on the used bonding method. A schematic overview is shown in Figure 15.

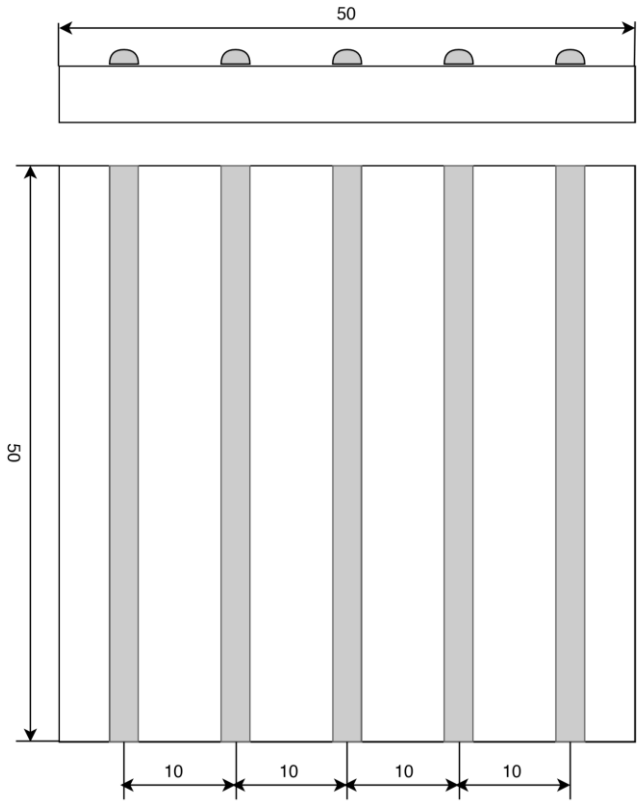

Figure 15: Schematic overview sample layout

3.3 Bonding methods

3.3.1.1 Ultrasonic welding

Ultrasonic welding uses a welding tool with ultrasonic vibrations and an external pressure which creates a connection between substrate and ribbon. The working principle is explained more in detail in section 2.2.1.

The ultrasonic welds are made with an ultrasonic welding tool from Schunk Sonosystems GmbH, type DS-35. This tool has the possibility to make welds with a maximum power of

800 watt by a working frequency of 35 kHz. Further, pressure, amplitude and welding energy can be changed.

The ribbons which are connected to the samples are made from aluminium. The width of these ribbons is 2 mm and the thickness 0,150 mm. Each ribbon is bonded on 8 spots as seen in Figure 16.

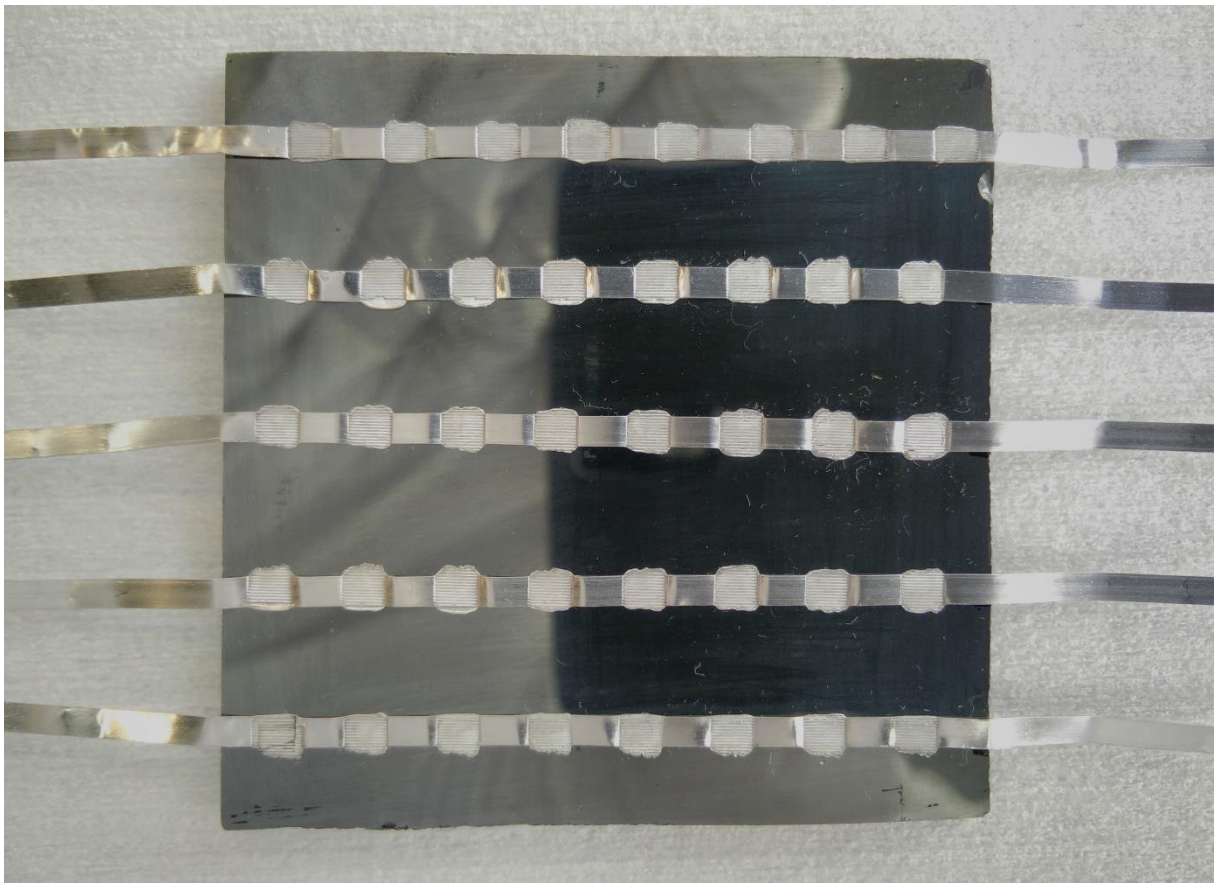

Figure 16: Ultrasonic welding sample on $MoSe_2$

Depending on the substrate material, the parameter settings vary to get an optimal connection. For ultrasonic welding, these parameters are determined empirically. The used parameters for the Mo and $MoSe_2$ bonds are shown in Table 2.

Table 2: Parameter settings ultrasonic welding

Substrate material	Pressure [bar]	Amplitude [%]	Energy [Ws]
Mo	3	75	20
$MoSe_2$	4	75	25

Before creating multiple samples with the optimal parameters, the influence of each parameter has been studied. The pressure varies depending on the materials used. 3 bar is enough to create bonds on the molybdenum samples while this pressure was not high enough to attach aluminium ribbons on $MoSe_2$ substrates.

The amplitude is kept constant on 75 %. Raising the amplitude to 100 % (no damping) resulted in bonds whereby the bond area became wider than the ribbon width. On the other hand, damping the amplitude below 75 % resulted in bonds whereby the ribbon did not connect to the substrate.

The last parameter influencing the bonds is the added energy. This parameter did not influence the shape of the bonds. The energy for bonds needs to be at least the values as described in Table 2 but raising the energy did not improve the bonding quality.

3.3.1.2 Ultrasonic soldering

Ultrasonic soldering is a bonding technique whereby the soldering tool can transfer ultrasonic vibrations through the heated solder. The ultrasonic vibrations replace the chemical flux which is used in traditional soldering applications. A more detailed explanation is done in section 2.2.2.

The tool which is used to create the solders on the samples is the USS-9210 from MBR Electronics GmbH. This soldering tool can regulate the temperature between 150 – 480 °C and the ultrasonic output power between 5 – 15 W by a frequency of 60 kHz ± 3 kHz.

The ribbon material is an alloy of tin, bismuth and silver. The dimensions are 0,08 x 1,6 mm. The used solder is #GS217 with a diameter of 1,0 mm which is a lead-free solder from CERASOLZER.

By the ultrasonic soldering process two elements are investigated. First, which are the optimal parameters and secondly, how to make the connection. The parameters for ultrasonic soldering are empirically determined. The following settings are used for both substrates (Mo and $MoSe_2$):

- temperature: 440 °C;
- ultrasonic power: 13.5 W.

Secondly, the way of attaching the ribbon is investigated. The first method tried was soldering the ribbon directly to the substrate with no solder layer in between. This method did not work because the solder on the tooltip did not flow between substrate and ribbon.

To solve this problem the soldering process is done in two steps. First, the solder is attached to the substrate. Afterwards, the ribbon is connected on top of the solder. Hereby, two methods are tested:

- solder over the full length where the ribbon is attached to the substrate;
- solder only on certain spots with a fixed distance in between.

Based on mechanical strength, the connections whereby the ribbon was soldered over the whole length are more rigid. Another advantage is that the contact surface is larger which results in higher conductivity. A sample whereby the ribbons are ultrasonic soldered over the whole length of the ribbon is shown in Figure 17.

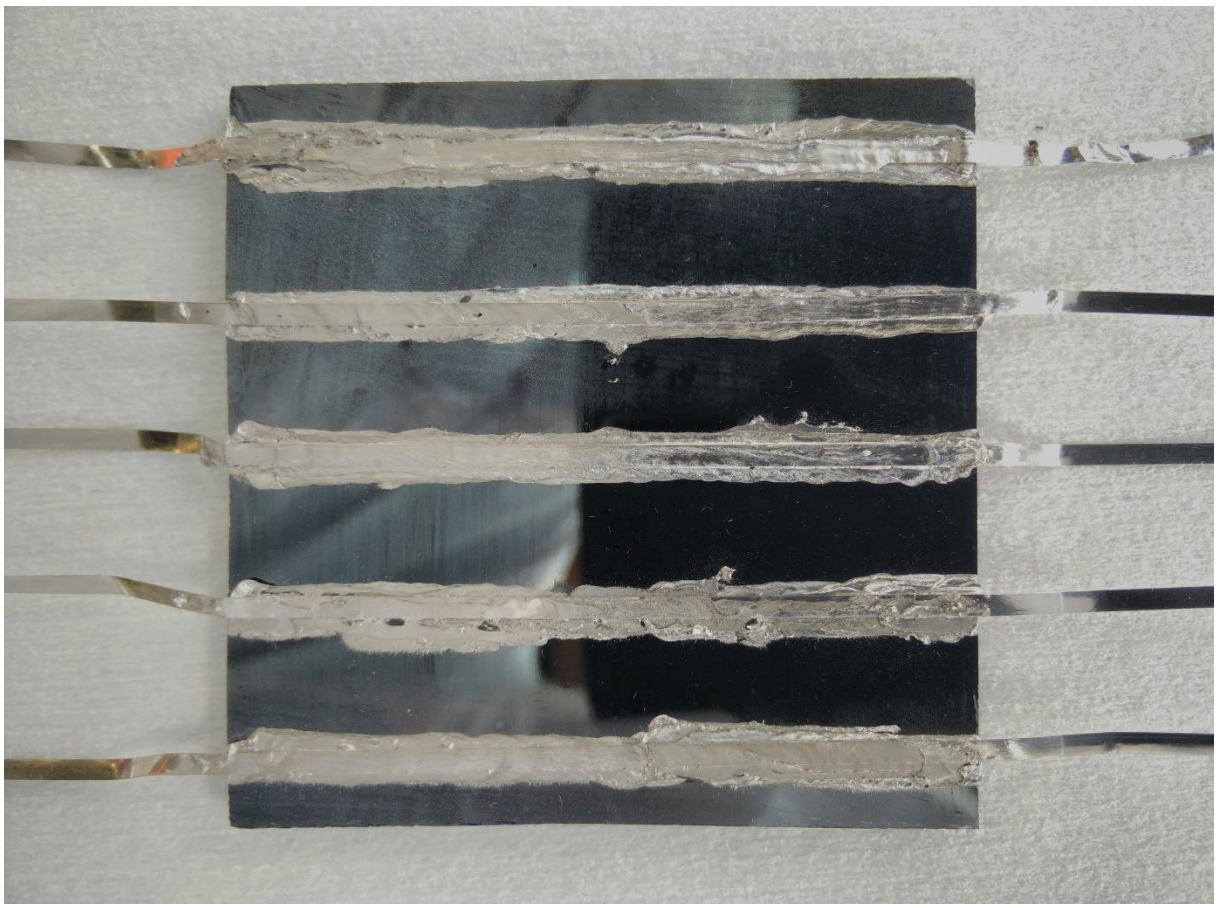

Figure 17: Ultrasonic soldering on $MoSe_2$ sample

The ribbons are manually soldered to the substrate. As a result, the distances between the ribbons is not the same for each sample. This must be taken into account when determining the contact resistances using TLM.

3.3.1.3 Electrically conductive tapes

In this master's thesis two electrically conductive tapes are tested. The most important difference between these two tapes is the used adhesive. One tape uses an electrically conductive adhesive as described in section 2.2.3. The other tape uses a non-conductive adhesive.

3M 1181 Conductive Copper Tape has conductive particles in the adhesive which creates the electrical connection between the copper foil and substrate. The width which is used in this application is 6.4 mm.

3M Embossed Copper Foil Shielding Tape 1245 has a groove pattern in the conductive metal layer which presses through the non-conductive adhesive to make an electrical contact. The tape width is 6 mm.

The tapes are shown from above in Figure 18. The 3M 1181 is on the sample on left side of the picture. On the right side is a sample with the 3M 1245 tape attached. The 3M 1245 tape can be recognised by the pattern.

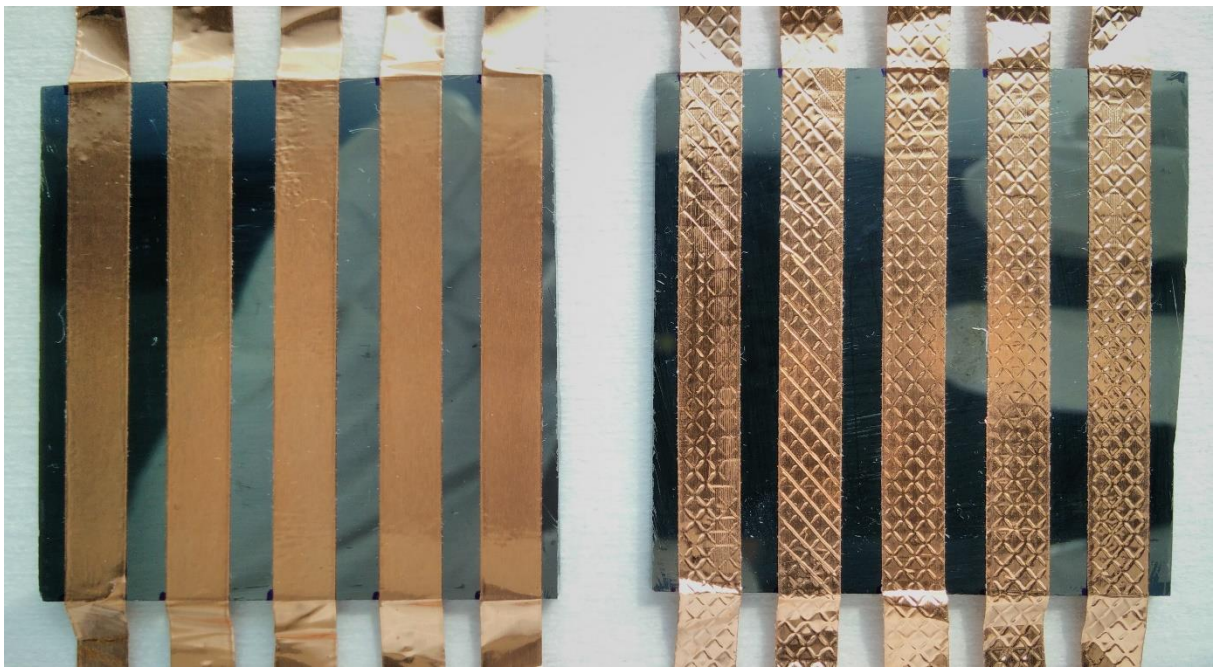

Figure 18: Electrically conductive tapes: 3M 1181 (left) and 3M 1245 (right)

To apply a uniform pressure on the tape's whole surface and each sample, a laminator is used. With the use of the laminator, the tape is attached to the sample with a pressure of 1 bar and a temperature of 25 °C for 60 seconds.

3.4 Degradation methods

Photovoltaic solar panels have an expected lifespan of approximately 20 years. To measure the degradation of the solar panels in a smaller period (i.e. 40 – 50 days), degradation methods are used. As mentioned in section 0, these stress tests are specified in the IEC 61646 norm for thin-film photovoltaics.

The next sections describe where the used stress methods are different from the test specified in the norm.

3.4.1.1 Damp heat test

The first test that is used to accelerate degradation is damp heat. The conditions are the same as specified in the norm, which are a temperature of 85 °C with a relative humidity of 85%.

The difference with the norm is the duration. The norm specifies 1000 hours of exposure. Instead the samples with the interconnections were exposed for almost 500 hours. The measurement interval was once per 24 hours on weekdays.

Beside the duration, the bonds on the samples are directly exposed to the testing conditions. This is in contrast to the norm where complete solar panels are tested. In complete solar cells the connections are sealed. Thus, the expectation is that the samples will degrade faster than in complete solar panels.

3.4.1.2 Thermal cycling

A second stress test which is used is thermal cycling. The temperature varies as specified in the norm between -40 °C and +85 °C. The difference is the duration of one cycle, the total duration is 3 hours while the norm specifies cycles of maximum 6 hours.

3.5 Characterization methods

To make a comparison between the different bonding techniques are characterised. The first comparison method is based on the contact resistance. Reducing the contact resistance leads to lower power losses in photovoltaic solar panels.

Secondly, SEM-images are made when delamination occurs after stress testing the samples. There will be a pre-test and post-test image to investigate which layers delaminate from each other.

3.5.1.1 Contact resistance measurements

The contact resistance is determined via the transmission line model which is explained in section 2.4.1. The resistance measurements are done with the Keithley 2000 Digital Multimeter using the four-wire resistance function.

To determine the contact resistance, four resistances are measured. The resistance between the following ribbons is measured:

- ribbon 1 and 2,
- ribbon 1 and 3,
- ribbon 1 and 4,
- ribbon 1 and 5.

This is schematically shown in Figure 19. The black cables are continuously attached to ribbon 1 while the red cables are changed to measure the different resistances.

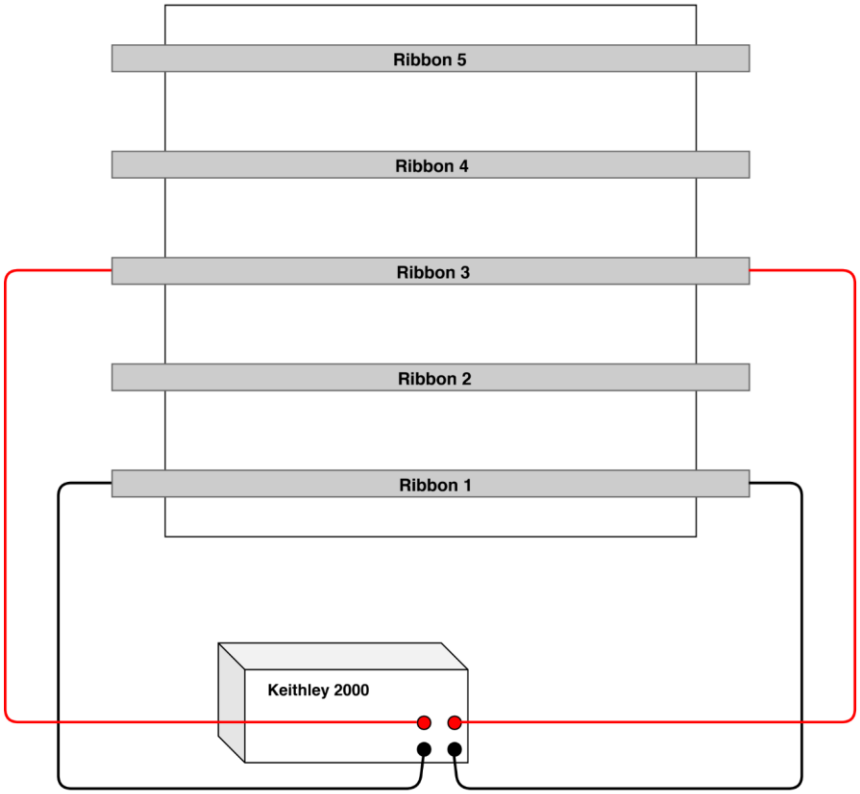

Figure 19: Connection diagram for four-wire resistance measurements

3.5.1.2 Scanning electron microscope

In addition to characterizing the contact resistance, SEM images were made. Images were made from initial samples and samples which were stressed due to damp heat because the most degradation occurred on damp heat stressed samples.

Two types of images were made: top view and cross section. Top view images were made to investigate the removal of the CIGS layer and to check the composition of the layer underneath which oxidized when ribbons were attached with USS.

Cross sections were made to inspect the connection between substrate and the conductive ribbon. Eventually, the location of any delamination can be investigated.

4 Results and discussion

4.1 Ultrasonic welding

4.1.1 Initial contact resistance

The first measurements made for characterizing the ultrasonic welds were the initial resistances to determine the contact resistance. These measurements have been done on 5 different Mo-substrates and 14 $MoSe_2$-substrates. The average values from both substrates are plotted in Figure 20.

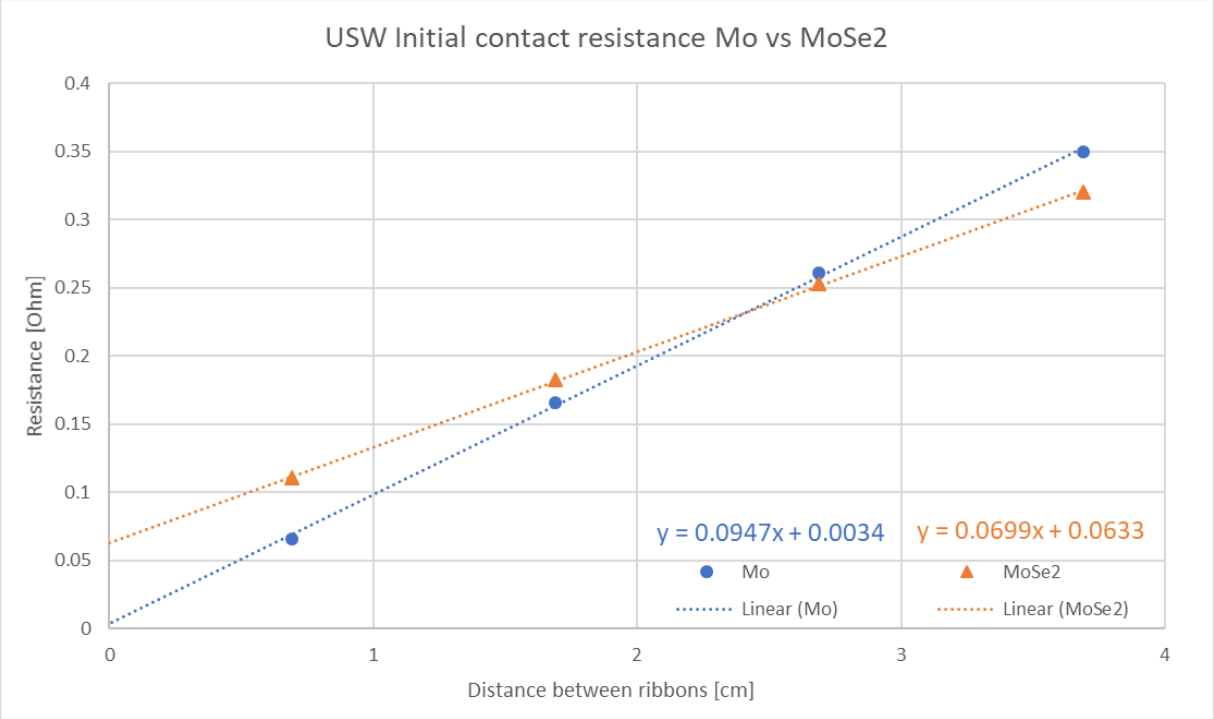

Figure 20: USW initial contact resistance

The distance used to plot the resistances is the difference between centre-to-centre distance and the width of the bond. For two adjacent ribbons is the distance 0.69 cm. The contact resistance for ultrasonic welds made directly on the molybdenum (1.6 mΩ) is almost 20 times lower than the ultrasonic welds made on the $MoSe_2$-substrates (31.65 mΩ).

The slope difference between the molybdenum and $MoSe_2$ samples is due to the difference in back contact layer thickness. The back contact layer on the $MoSe_2$ substrates is thicker than the molybdenum substrates. Because of this difference, the $MoSe_2$ substrates have a lower sheet resistance which results in flatter slope.

4.1.2 Degradation due to thermal cycling

Five $MoSe_2$-samples with ultrasonic welds have been thermal cycled. The resistances were measured once per day which is equal to 8 thermal cycles. After 92 cycles there was no significant degradation measured in comparison with the damp heat stressed samples whose results are shown in section 0. The R_c-development is shown in Figure 21.

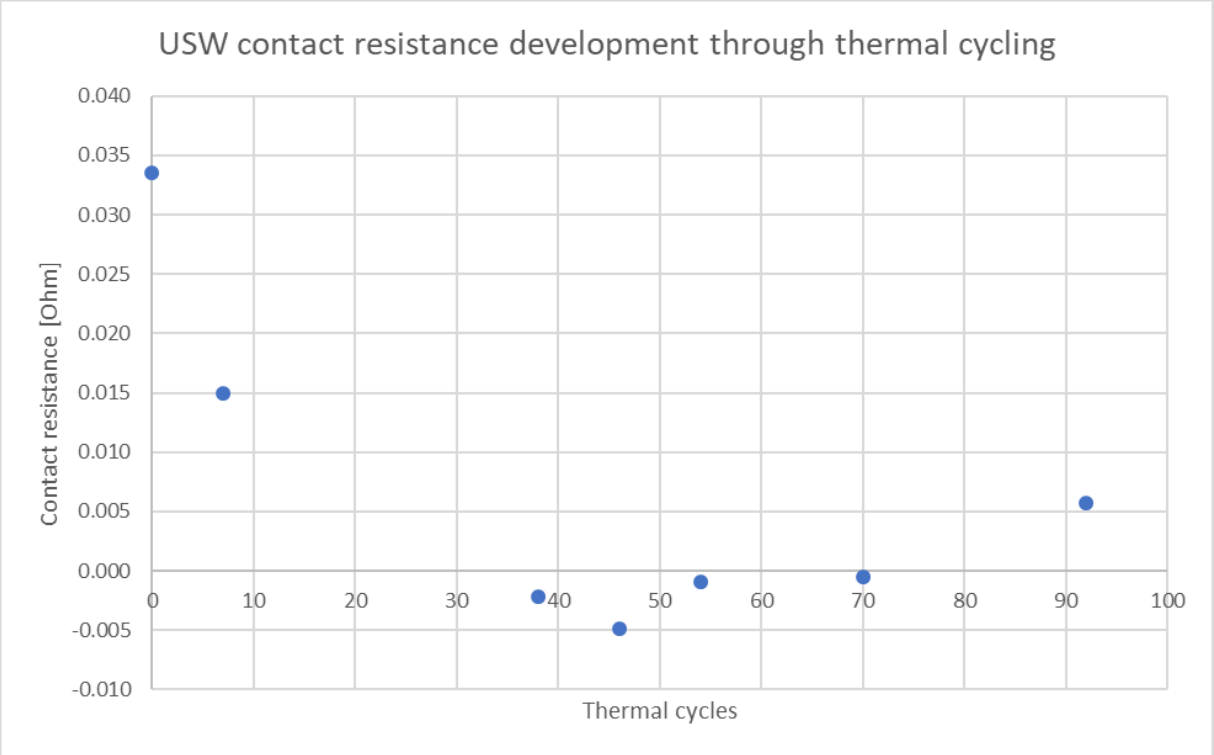

Figure 21: USW average contact resistance development due to thermal cycling

The first three measurements, the contact resistance was decreasing. This is probably due to an annealing process. Afterwards, the R_c remained reasonably stable from the 38th until the 70th cycle. At the last measuring point, after 92 cycles, the R_c raised with 7 mΩ.

4.1.3 Degradation due to damp heat

Five other $MoSe_2$-samples, which were not used for thermal cycling, were stressed for 492 hours damp heat. These samples also have been measured every 24 hours like the samples which were thermal cycled. As mentioned in 4.2.2, the measurement setup for the initial measurements was different than the setup for the rest of the measurements. This resulted in a negative offset relative to the initial contact resistance. The R_c-evolution is plotted in Figure 22.

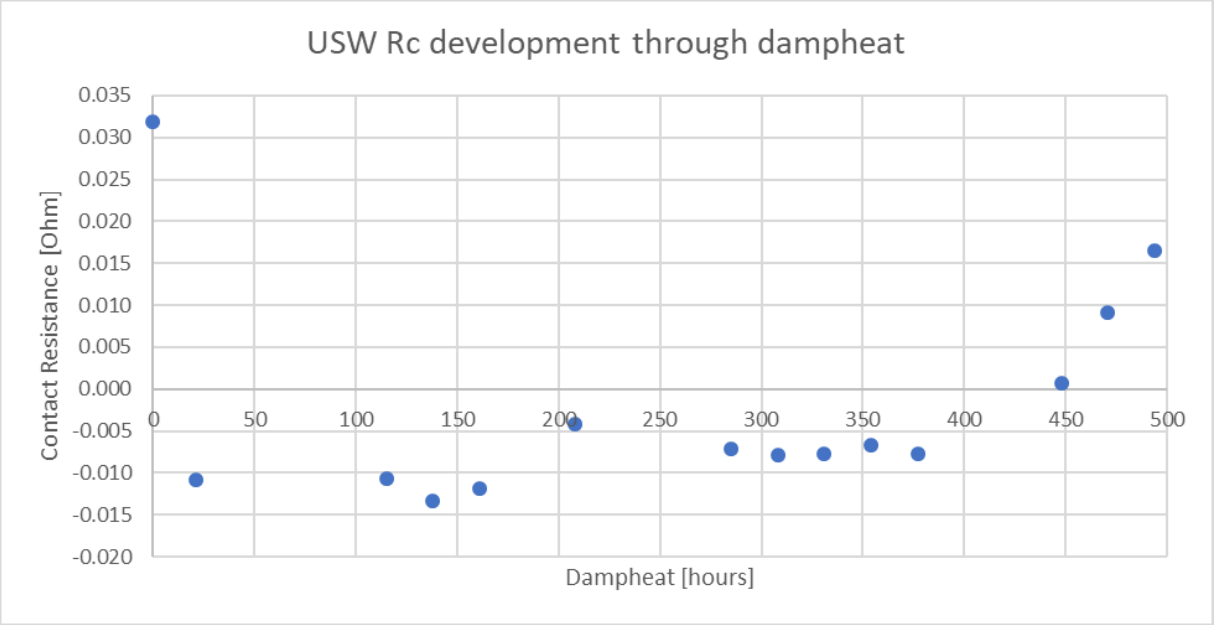

Figure 22: USW average contact resistance development due to damp heat

The average R_c-value remained quite stable for the first 380 hours. The next measurement (after 450 hours) the R_c raised with 9 mΩ. The last two measurements, the R_c raised again with 8 mΩ and 7 mΩ relative to the previous measurement.

4.1.4 SEM images

The first SEM image, shown in Figure 23, is a top view of an ultrasonic weld made on $MoSe_2$. Due to pressure of the ultrasonic welding device, the weld became wider than the ribbon itself.

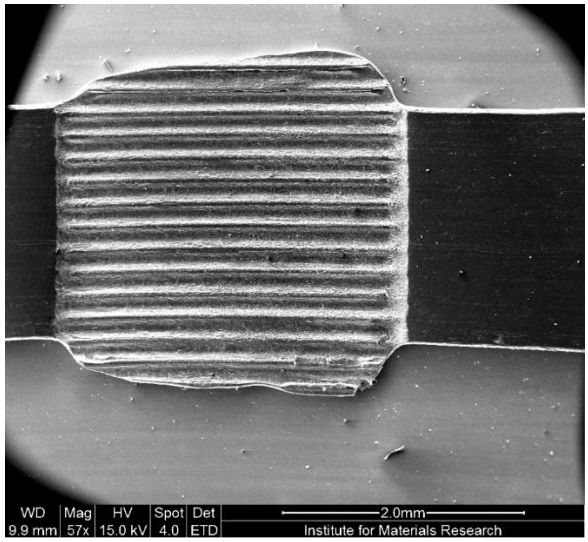

Figure 23: Top view ultrasonic weld on $MoSe_2$ made with SEM

The same area as in Figure 23 is inspected to make an energy dispersive X-ray (EDX) image, which is shown in Figure 24. The detected material in area 1 and 2 is aluminium from the ribbon. Area 3 is the substrate where the CIGS layer is removed. In this marked area especially molybdenum and selenium are detected, indicating that the $MoSe_2$ layer is present.

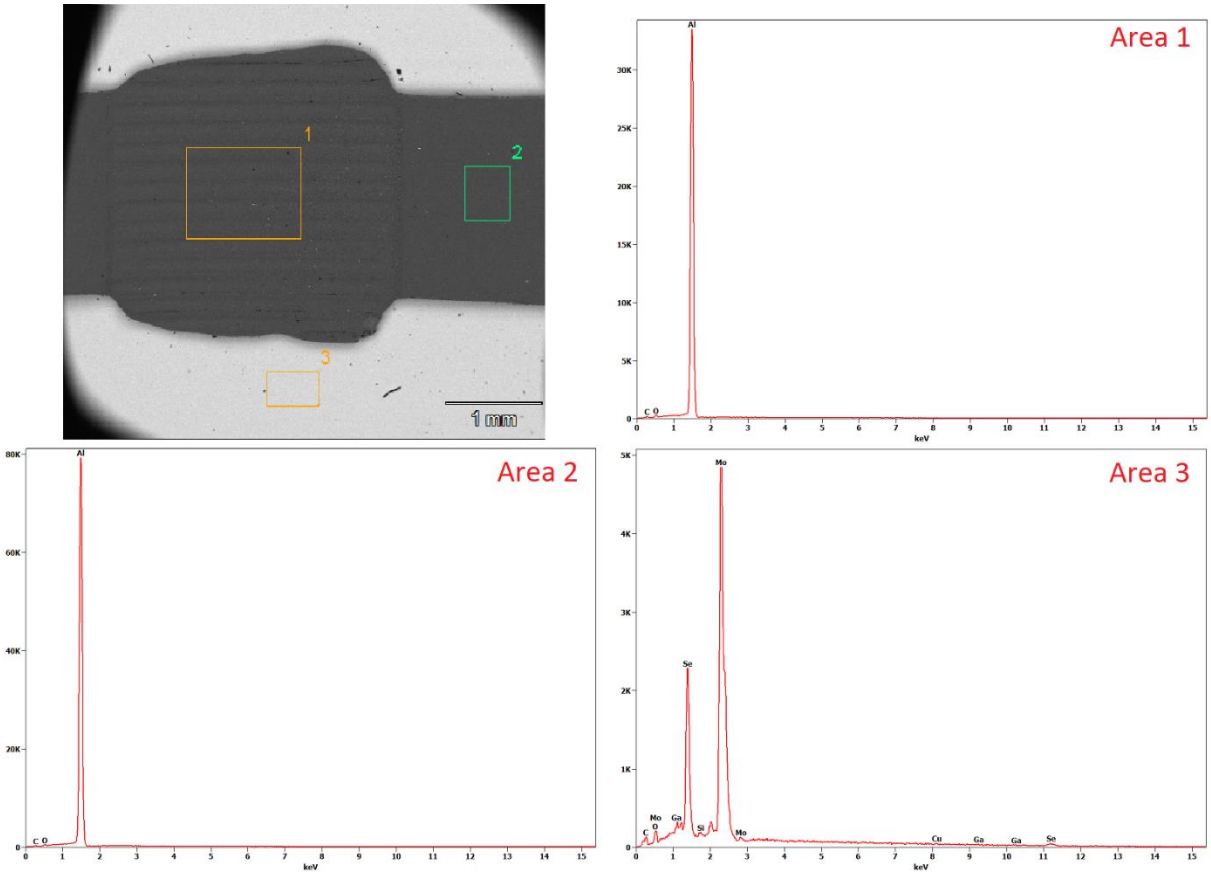

Figure 24: EDX top view ultrasonic weld on $MoSe_2$

A stressed sample was also inspected with the SEM after the damp heat test. These images were made from a smaller surface to examine the degradation. Figure 25 is a detailed $MoSe_2$ area on an ultrasonic welded sample which is damp heat stressed. Multiple points are indicated in this image. These points are numbered according to degradation level from no degradation to the most degradation. The detected materials from these points are presented in the charts in Figure 26.

Area 1 is not affected by the damp heat test. Next, in point 2 minimal degradation is visible because a little peak of oxygen is visible while selenium decreased. This indicates that $MoSe_2$ substrates with USW bonds also started to degrade. In point 3 selenium decreased even more. These observations are also visible in points 4, 5 and 6. But in these points, silicon is also detected which indicates that the back contact layer is also affected over time.

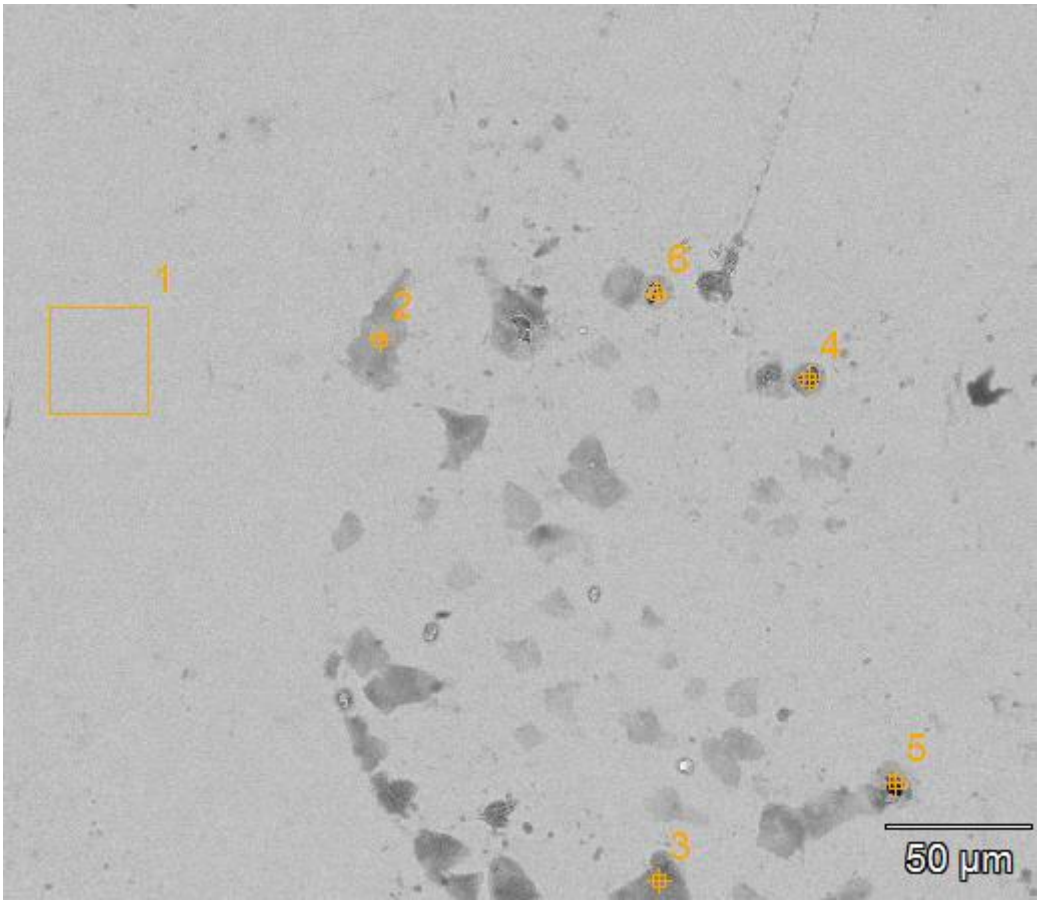

Figure 25: EDX top view $MoSe_2$ area on USW sample after damp heat stressing

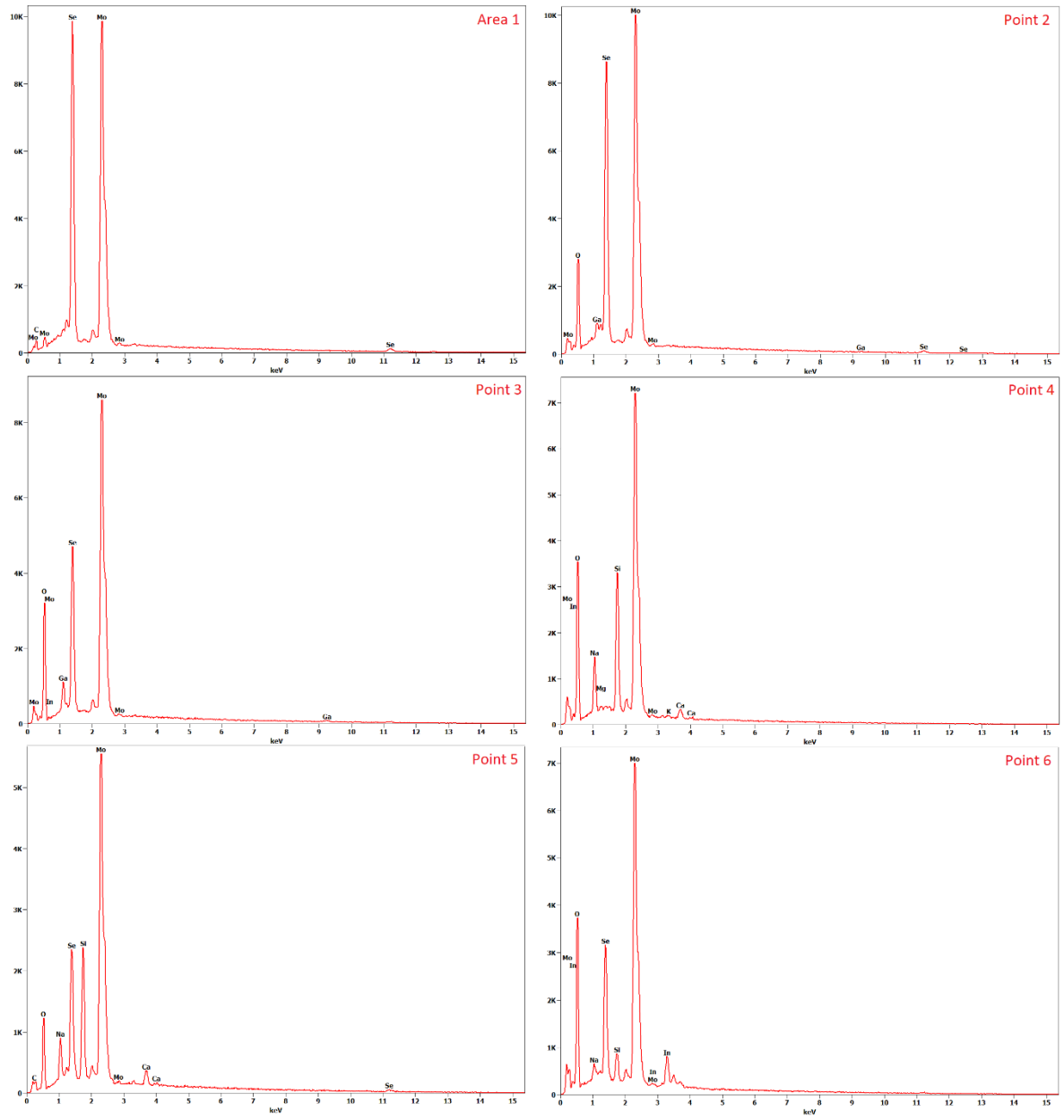

Figure 26: Detected materials from $MoSe_2$ area on USW sample after damp heat testing

Besides the $MoSe_2$ image, there was also an image made from the aluminium ribbon after the damp heat test. This image is shown in Figure 27. In this image there are three areas indicated. In areas 1 and 2, oxygen is detected in addition to aluminium. Though, in area 3 the oxygen part is very limited. The gray scale in area 3 can be seen on most of the image, indicating that the degradation on the ribbon is limited.

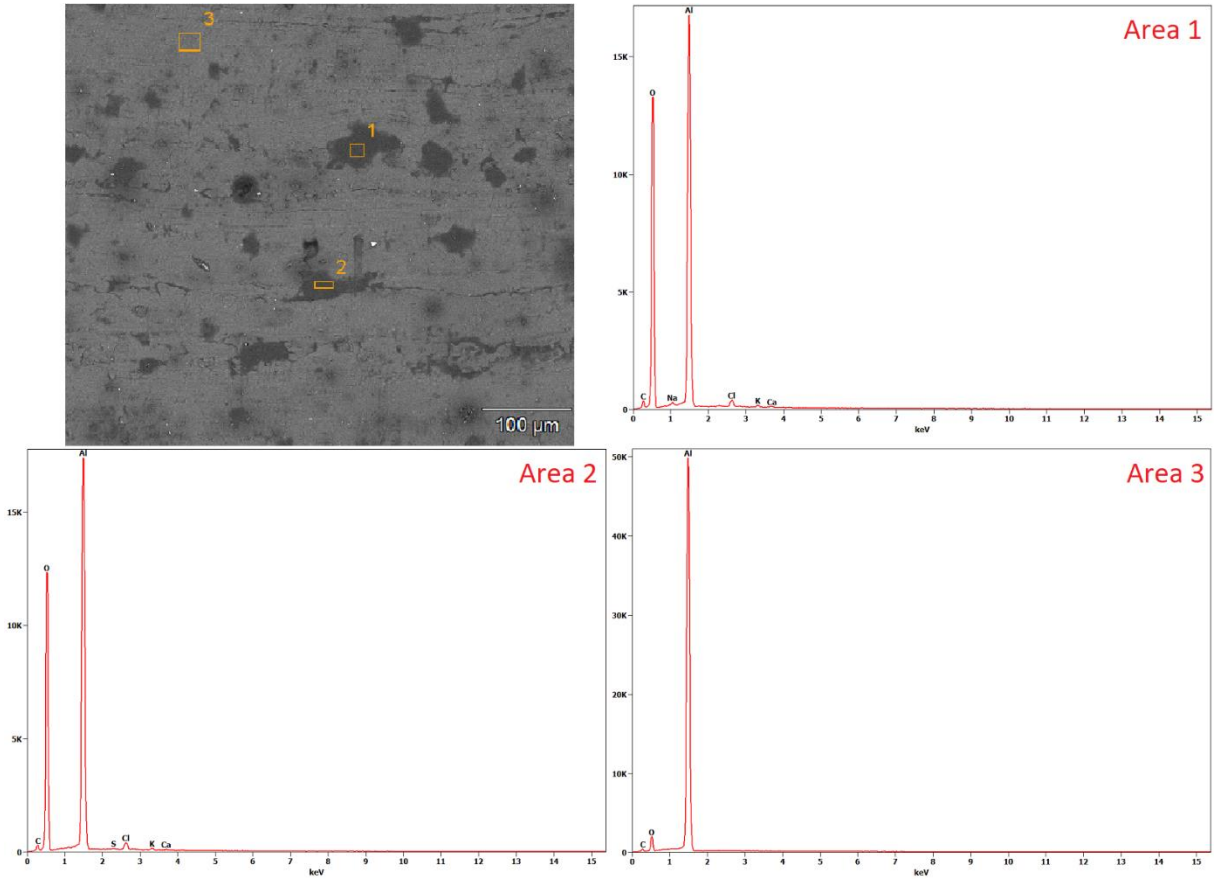

Figure 27: EDX top view aluminium ribbon area on USW sample after damp heat test

4.2 Ultrasonic soldering

4.2.1 Initial contact resistance

The first measurements made for characterizing ultrasonic soldering was a comparison between ultrasonic soldering on Mo-samples and $MoSe_2$-samples in initial state. Figure 28 shows the average resistances from both substrate materials which were used to determine the contact resistance.

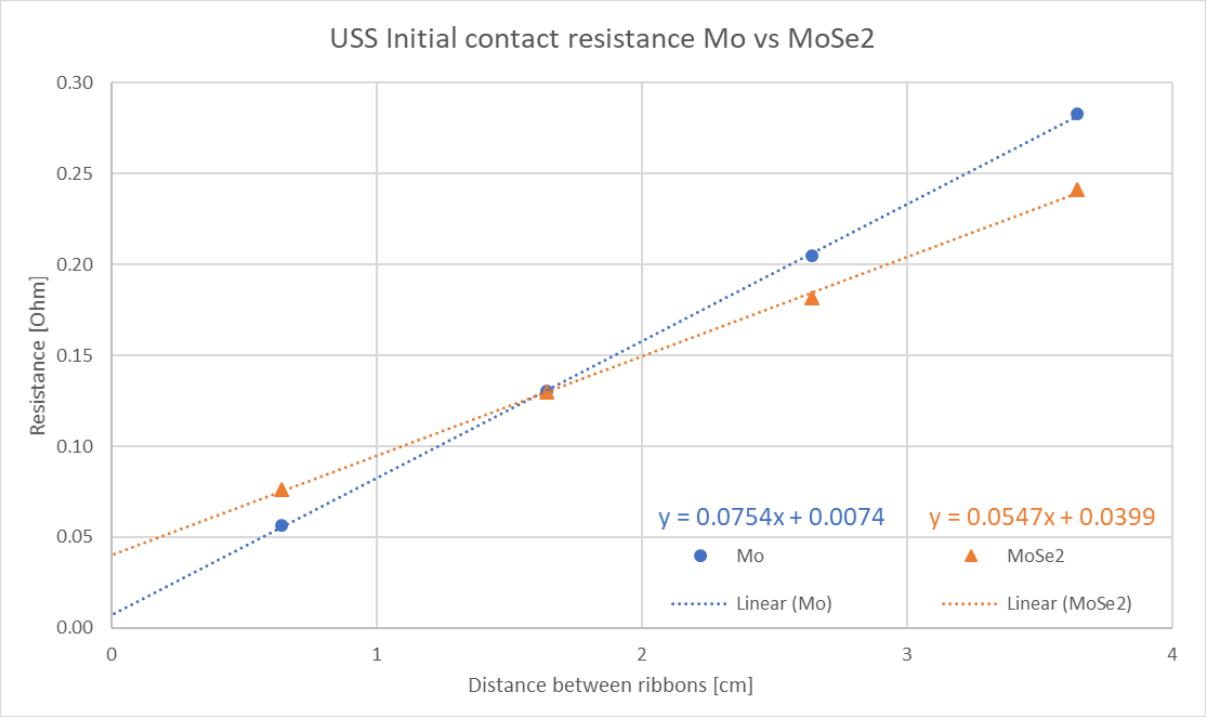

Figure 28: USS initial contact resistance

The average width of USS traces is 3.6 mm. With a centre-to-centre distance of 1 cm between two ribbons, the distance for two adjacent ribbons is 0.64 cm. Due to the absence of the resistive $MoSe_2$-layer, the R_c-value for Mo-substrates is lower than the R_c for $MoSe_2$-substrates.

4.2.2 Degradation due to thermal cycling

Together with the USW samples, five USS $MoSe_2$-samples were thermal cycled for 92 cycles. Due to a different measurement setup the initial determined contact resistance is higher than the rest of the determined contact resistances. The evolution of the contact resistances is shown in Figure 29. After 92 cycles, the R_c was not significantly increased.

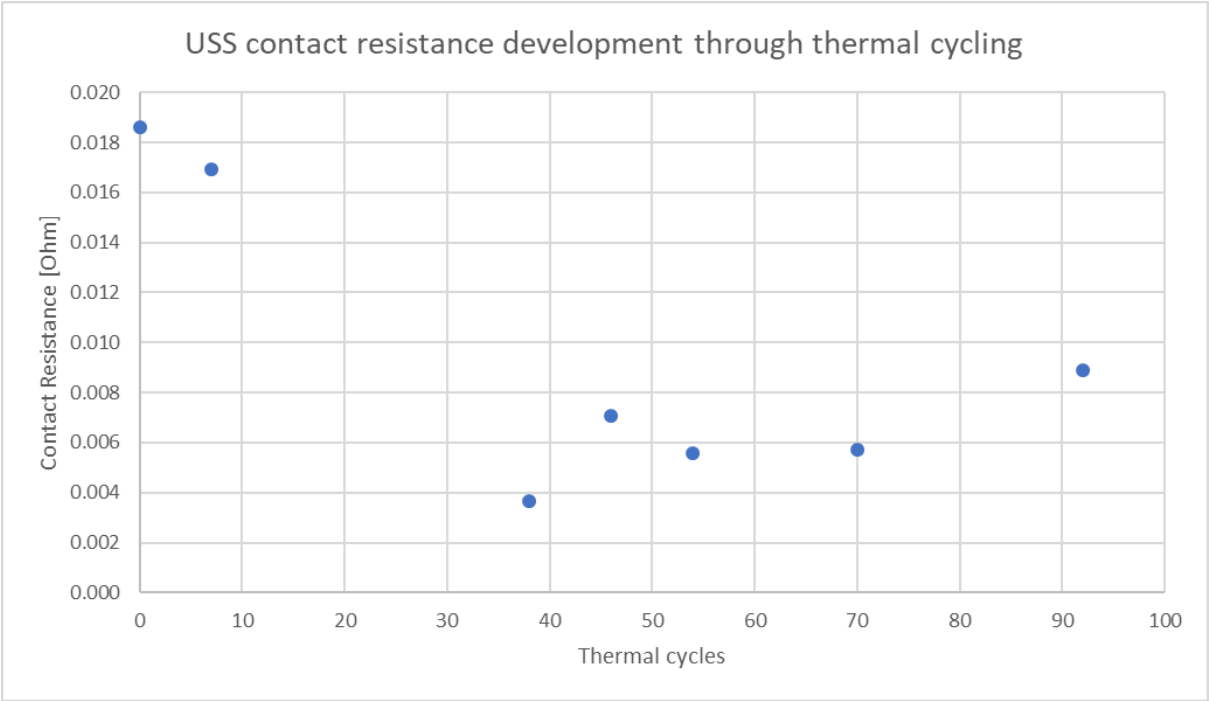

Figure 29: USS average contact resistance development due to thermal cycling

4.2.3 Degradation due to damp heat

Five ultrasonic soldered samples have been damp heat stressed for 492 hours. While running this test, the resistances from the samples were measured each 24 hours. The contact resistance remained reasonably stable the first 285 hours. Afterwards, the average R_c started decreasing instead of increasing which was expected. This evolution is shown in Figure 30. Around the same time multiple ribbons started to detach and seven ribbons were completely disjointed at the end of the test.

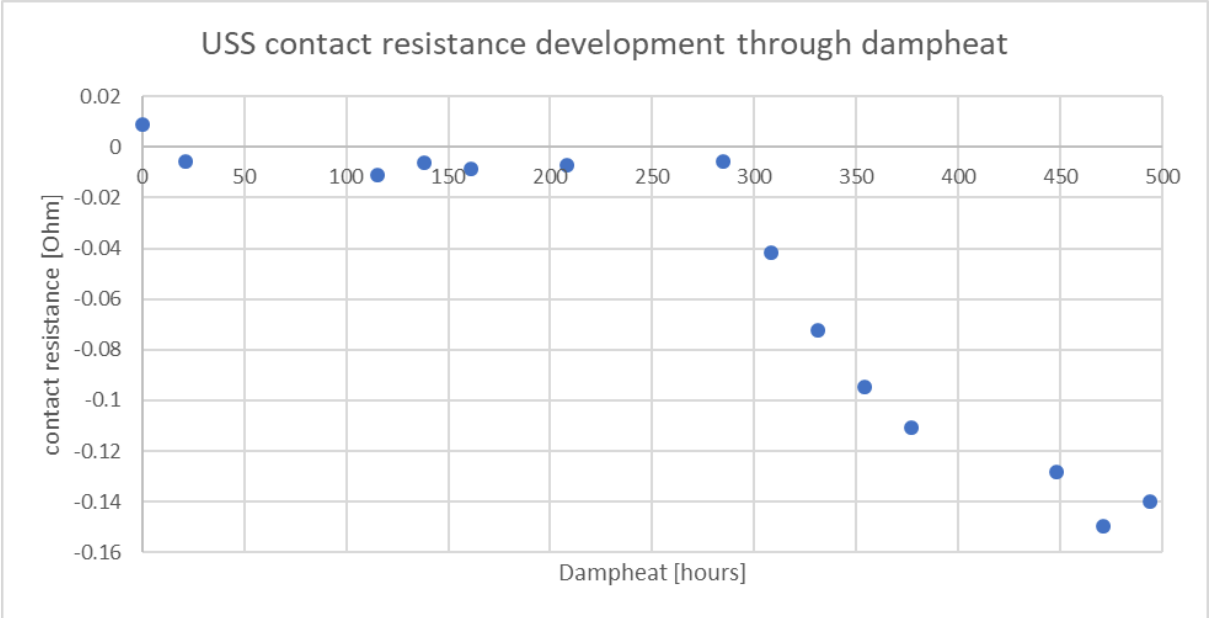

Figure 30: USS average contact resistance development due to damp heat

The cause for this evolution is that the resistance between ribbon 1 and 5 increased relatively harder than the resistance between ribbon 1 and 2 during the damp heat tests. As a result, the slope of the linear trendline became steeper which is shown in Figure 31. When the R_c is

determined using the TLM, it is negative. The hypothesis for this observation is that besides degradation on the interconnection, degradation also occurred on the substrate. This hypothesis is further investigated in sections 4.2.4 and 4.2.5.

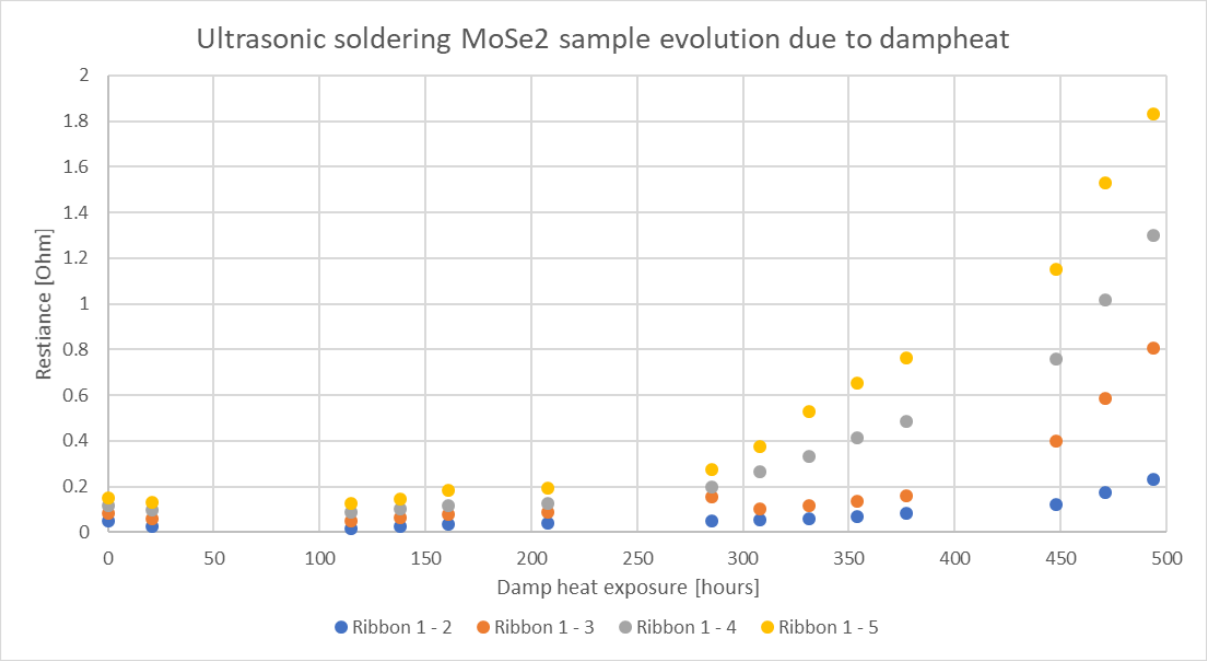

Figure 31: USS resistance evolution due to damp heat stress testing

4.2.4 SEM images

To begin with, an ultrasonic soldered ribbon on $MoSe_2$ is shown in Figure 32. In this image the layer structure for attaching the ribbon can be seen. First, a trace is made with solder. Then, the ribbon is connected on the solder trace.

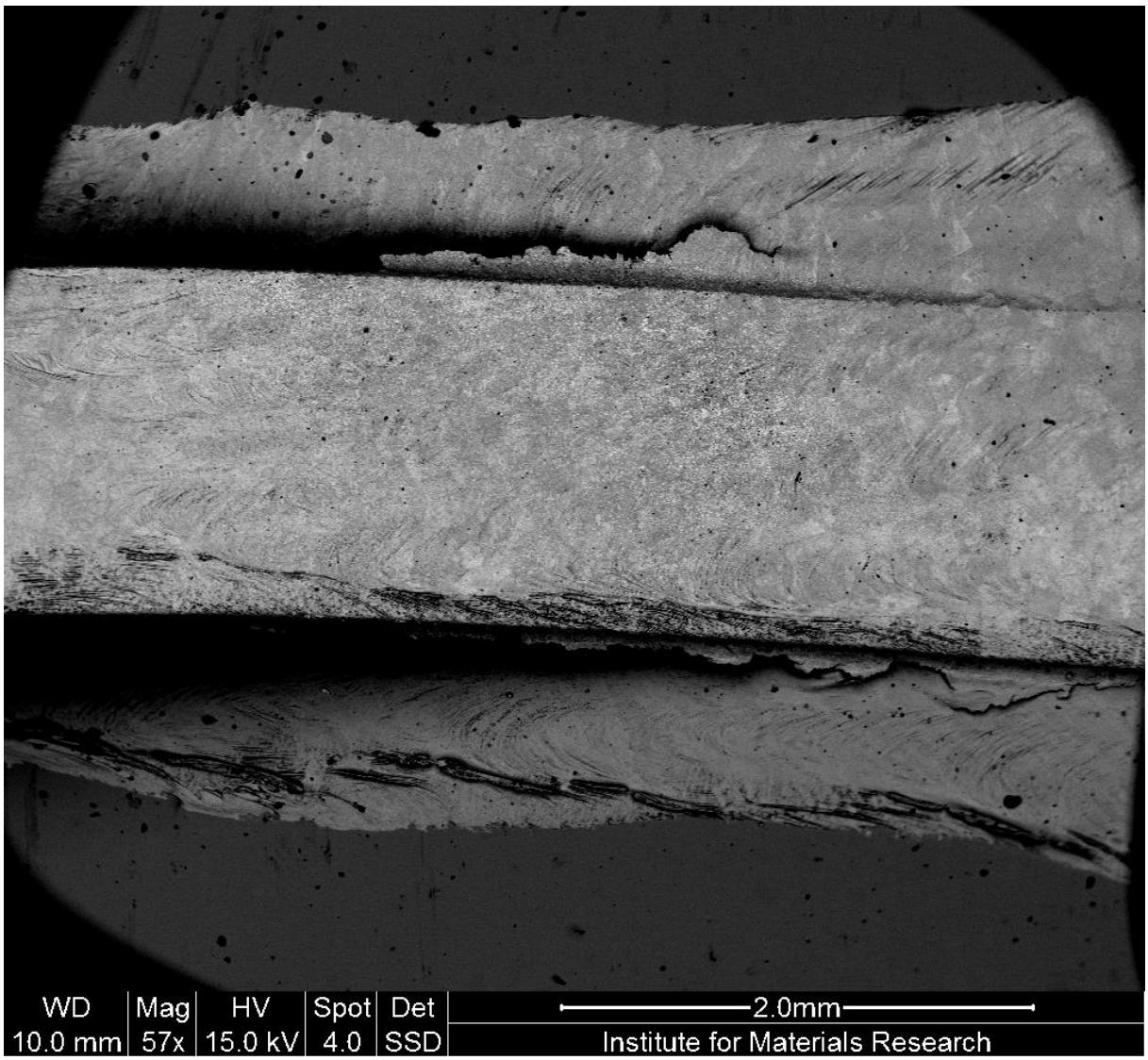

Figure 32: Top view ultrasonic soldered ribbon on $MoSe_2$ substrate

An EDX image was made from a more detailed section of the sample which is displayed in Figure 33. The upper part of the image is from the solder trace. The lower part is the $MoSe_2$ layer. This is confirmed by checking the materials in the marked areas 1 and 2. Area 1 mainly contains tin which indicates it is the flux free solder.

Area 2 consists for the biggest part of molybdenum while selenium is expected also. The ultrasonic soldering process affected the whole $MoSe_2$ layer. Point 3 has a deviating colour relative to area 2 but still consists mainly out of molybdenum. The $MoSe_2$ layer disappeared after attaching the ribbons with the USS method. Figure 34 is a top view image from a clean $MoSe_2$ sample whereby only the CIGS layer was removed. This substrate contains both molybdenum and selenium which indicates the presence of the $MoSe_2$ layer before ultrasonic soldering.

The $MoSe_2$ layer is also visible in the cross section image in Figure 35. Area 1 in Figure 36 shows the detected materials, which are mainly selenide and molybdenum, in the corresponding marked area in cross section image. The thickness of this layer is less than 0.4 μm. Below this layer is the molybdenum back contact layer which has a thickness of 0.5 μm.

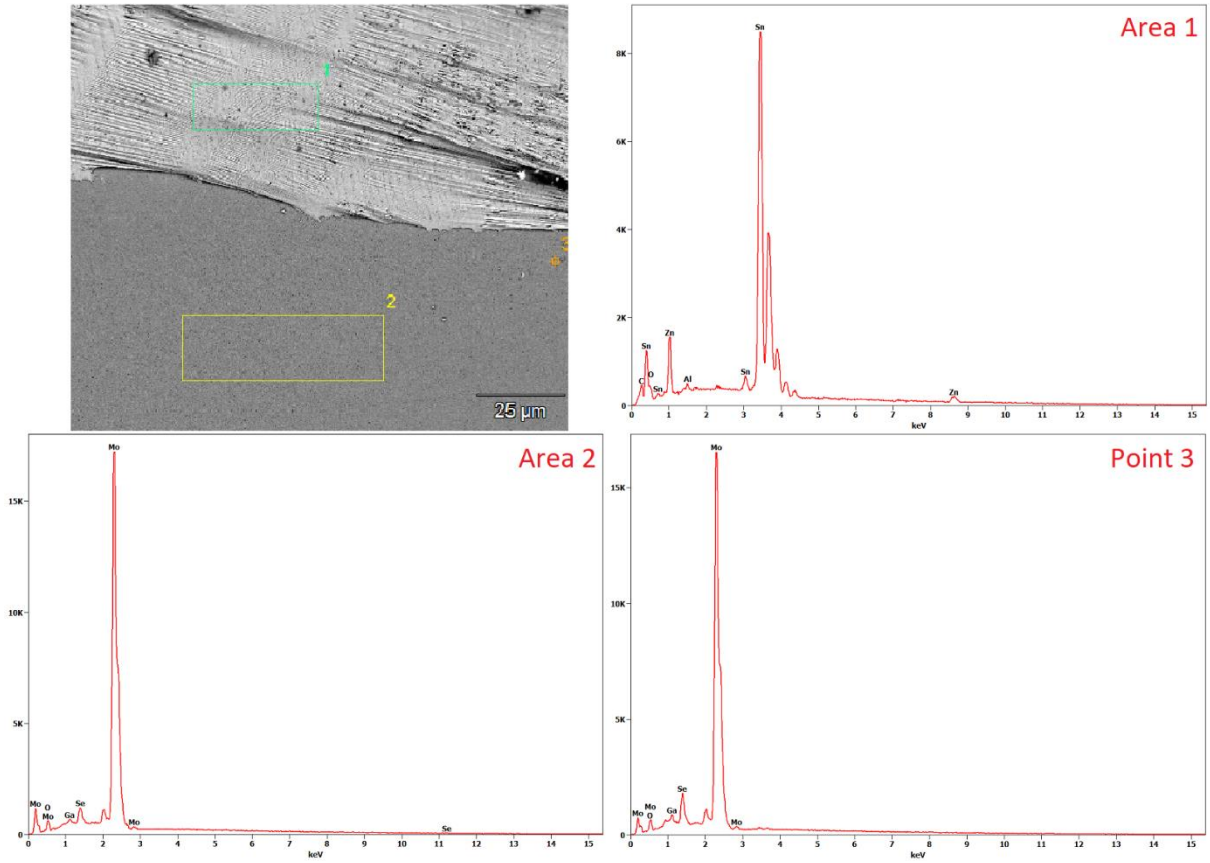

Figure 33: EDX top view ultrasonic soldering on MoSe2

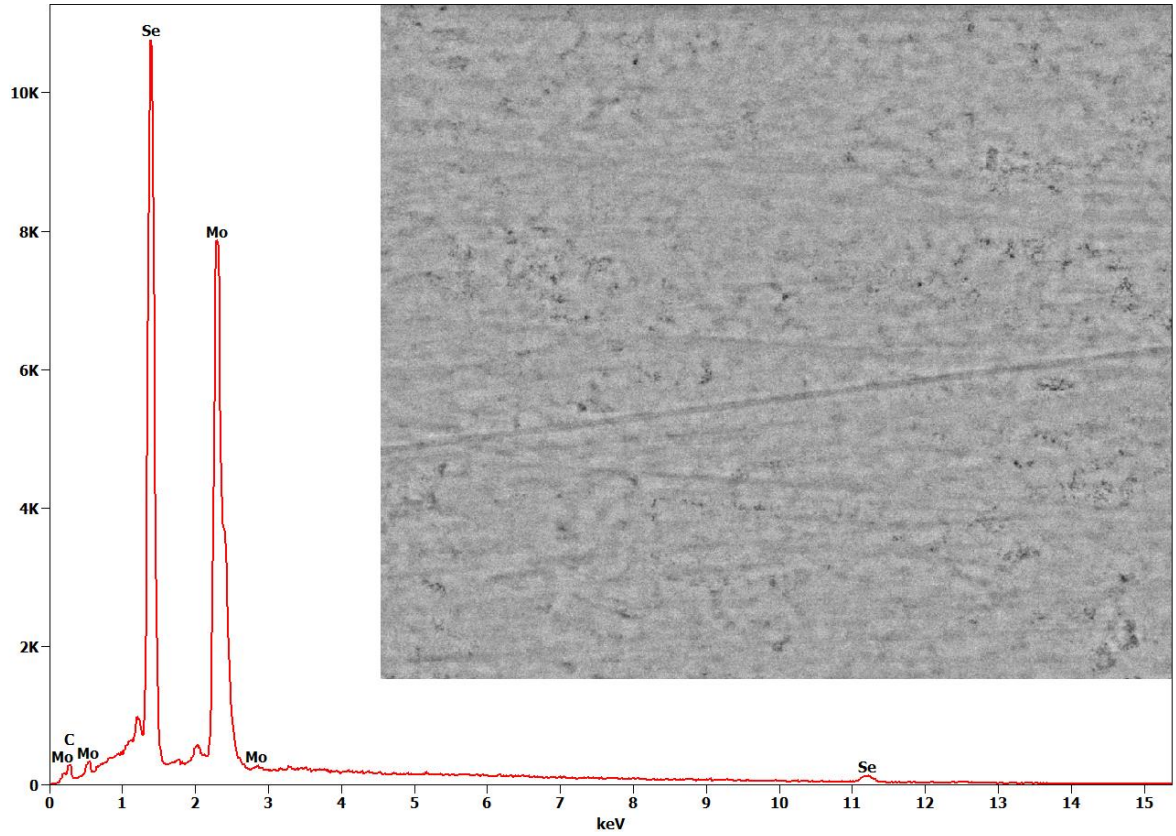

Figure 34: EDX top view pristine $MoSe_2$ substrate

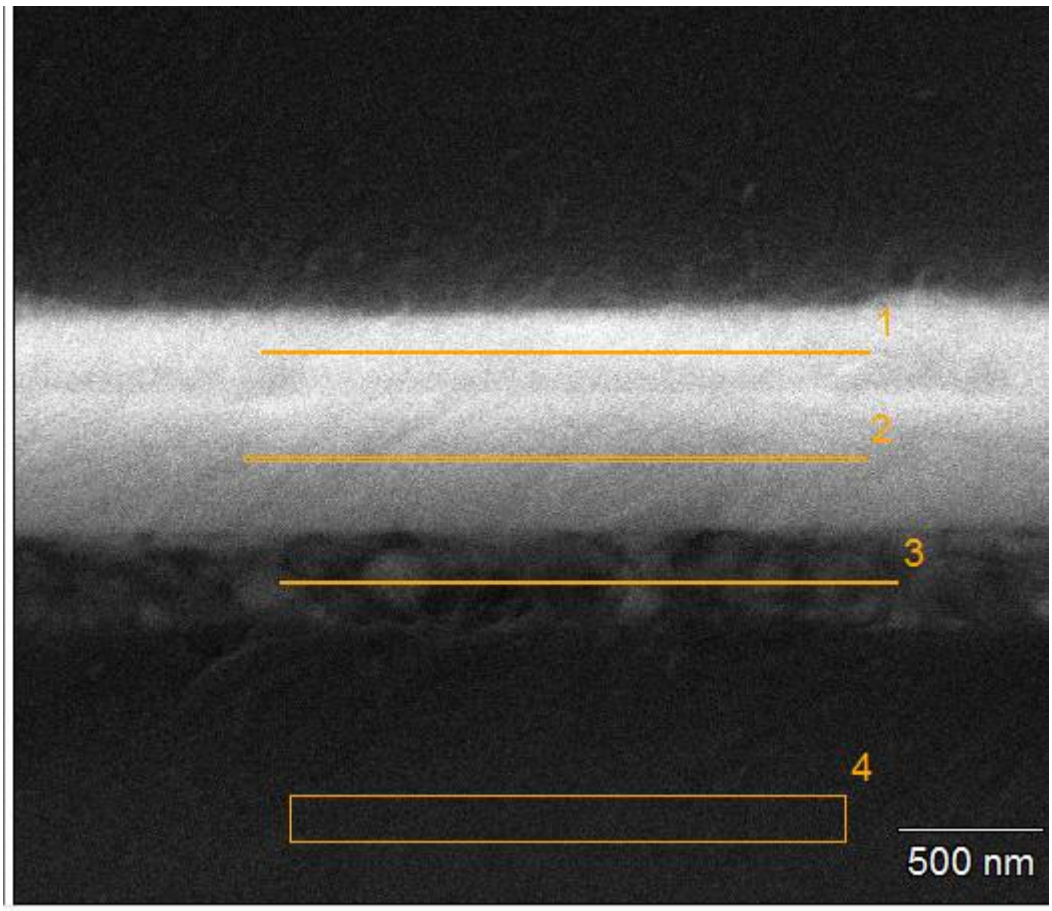

Figure 35: EDX cross section pristine $MoSe_2$ substrate

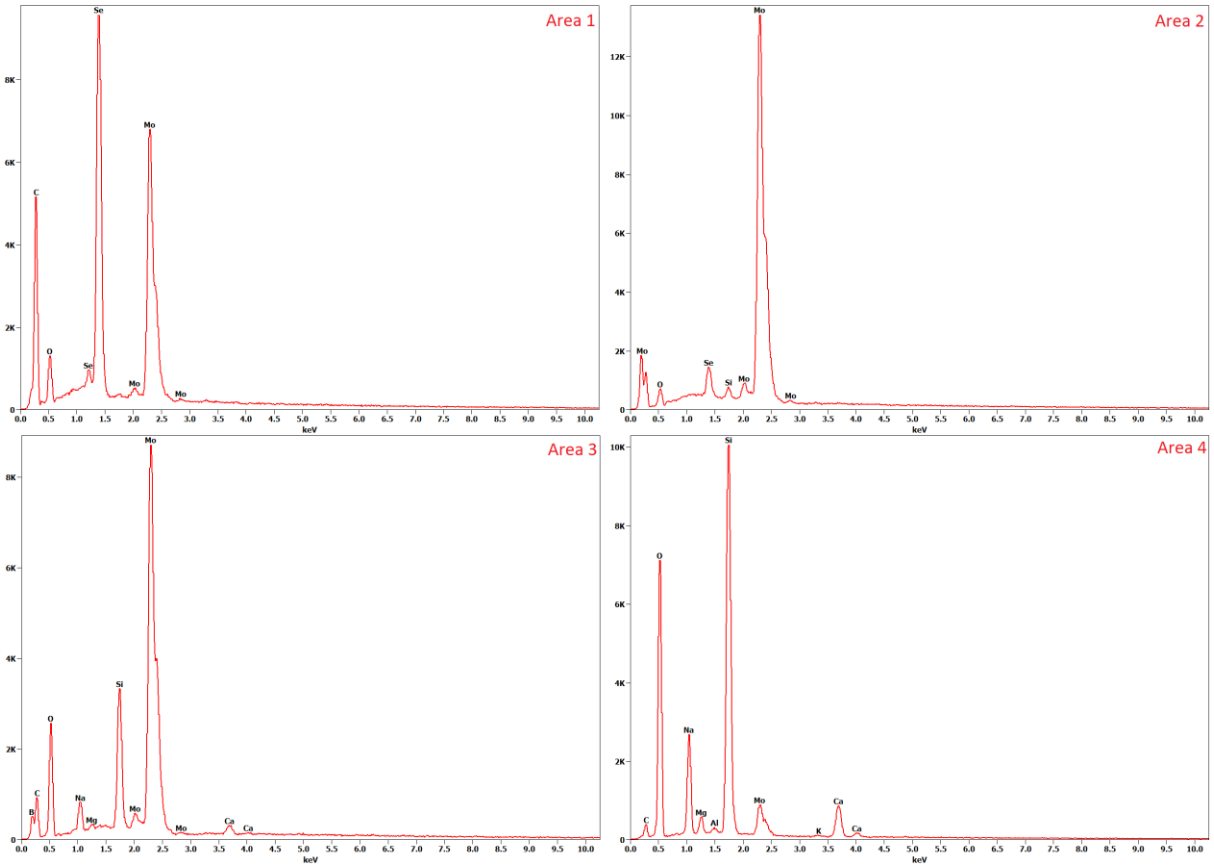

Figure 36: Detected materials pristine $MoSe_2$ sample in cross section

In Figure 37 a similar area as in Figure 33 is scanned with the SEM. There are two differences:

- the image in Figure 37 is from a sample which is stressed with damp heat;
- in the bottom half is the substrate layer visible, but in this area was the solder and ribbon attached to the substrate.

Again, three areas are marked in Figure 37. Area 1 is a combination between molybdenum and solder which started to oxidize. Area 2 is on solder with less oxidation and without molybdenum. Lastly, is the substrate marked in area 3 whereby no oxide is detected. The ribbon and solder were detached after the damp heat test.

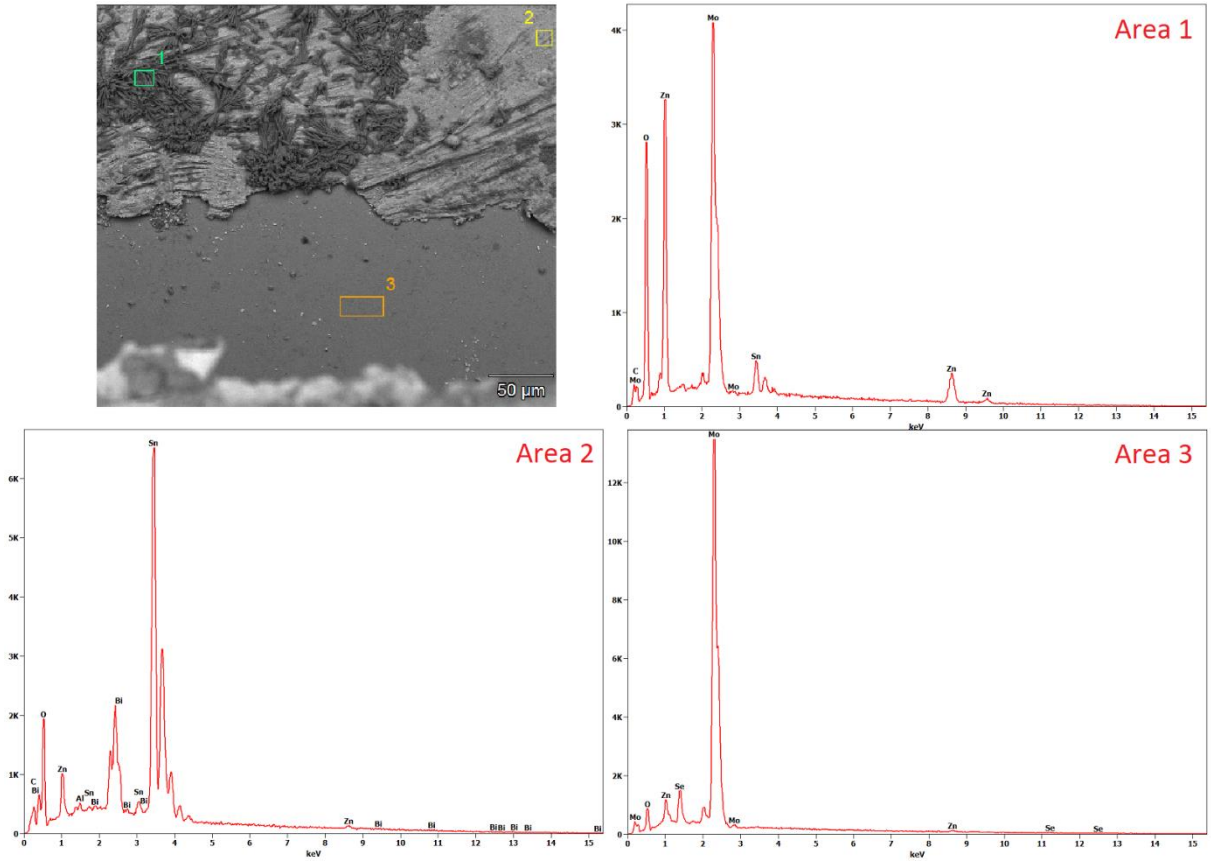

Figure 37: EDX top view ultrasonic soldering on $MoSe_2$ after damp heat

Figure 38 is an image from an USS $MoSe_2$ substrate area which is stressed with damp heat. The surface in this image is grainier in comparison with the bottom half of Figure 33. But areas 1, 2, 3 and point 5 contain mainly molybdenum and oxide. Area 4 is a remaining part from the absorber layer which was not removed.

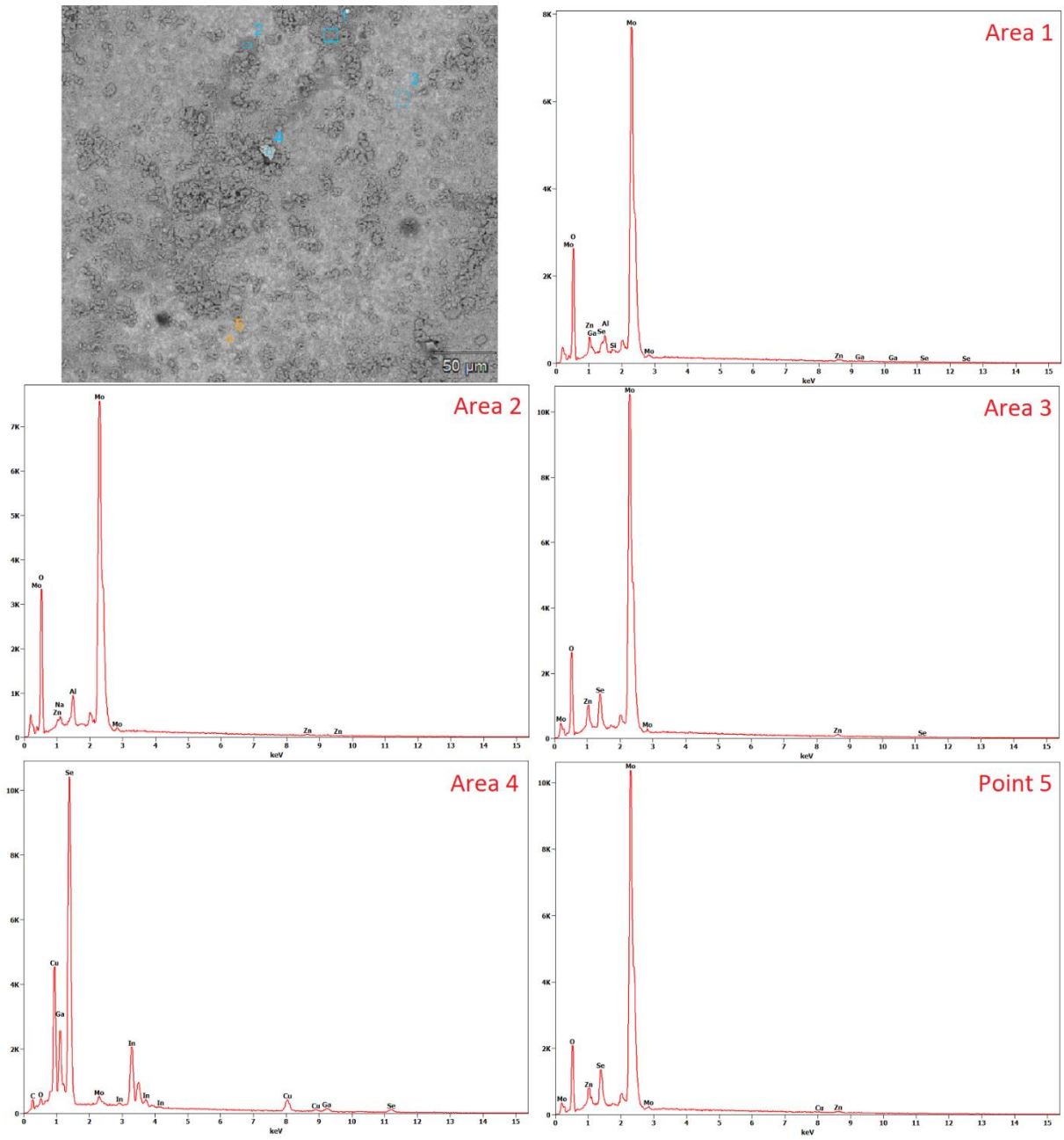

Figure 38: EDX top view ultrasonic soldered $MoSe_2$ substrate after damp heat

4.2.5 Optical images

The degradation which is seen in the SEM images from the previous section can also be seen in the optical images. When comparing an unstressed sample (Figure 17, p. 35) with stressed samples as shown in Figure 39, the colour change stands out on the substrate. Before stressing the substrates had a mirror effect. Afterwards, the samples became dull due to the damp heat testing.

Furthermore, the degradation is also visible at the backside of the samples. The entire back contact layer has been degraded, making the ribbons visible in some places on the back of the sample. This effect is visible in Figure 40. The image on the left side is a pristine sample where the back contact layer is completely intact. On the right image in Figure 40, the back contact layer is affected.

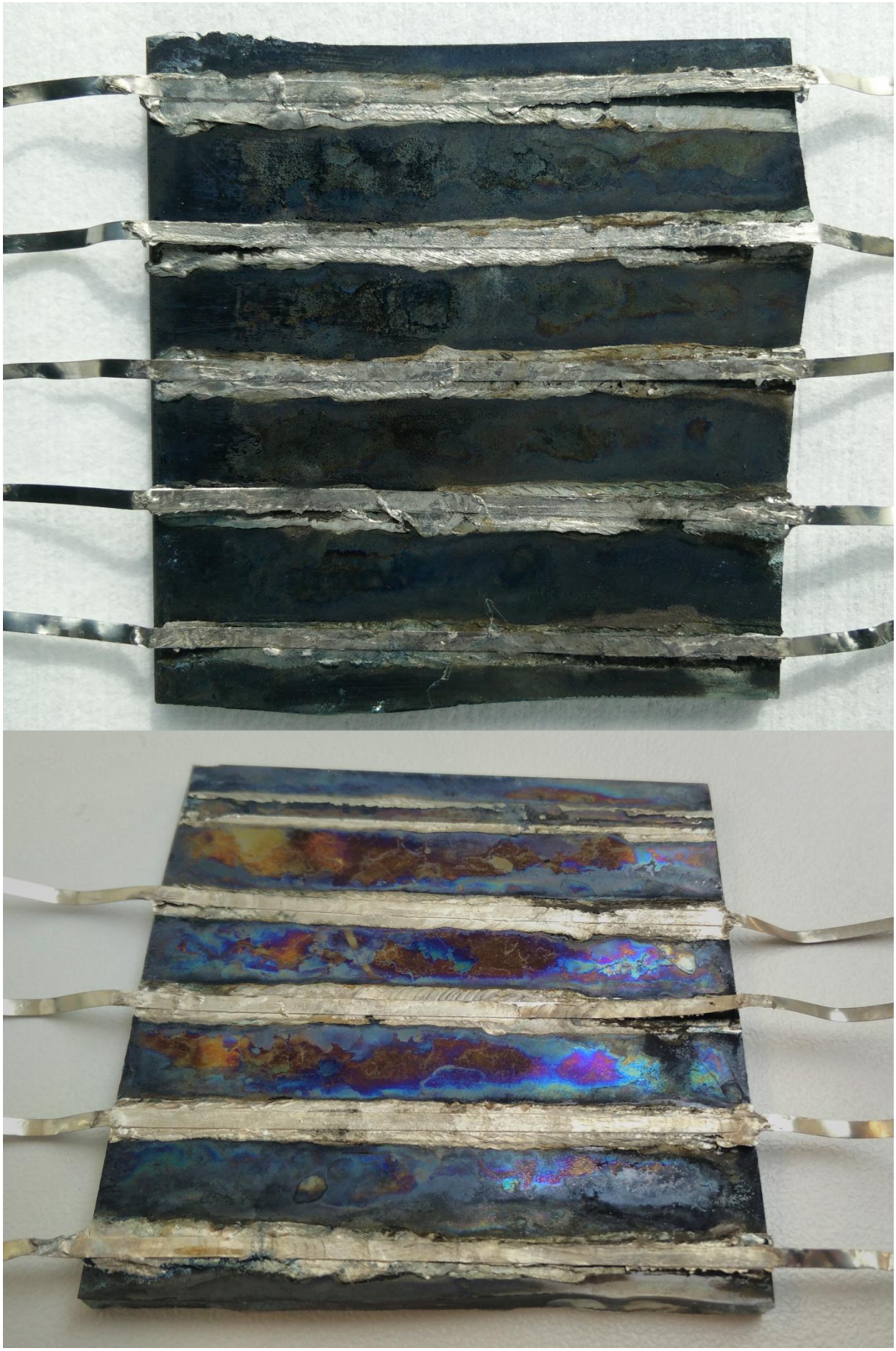

Figure 39: USS samples on $MoSe_2$ substrate after damp heat test

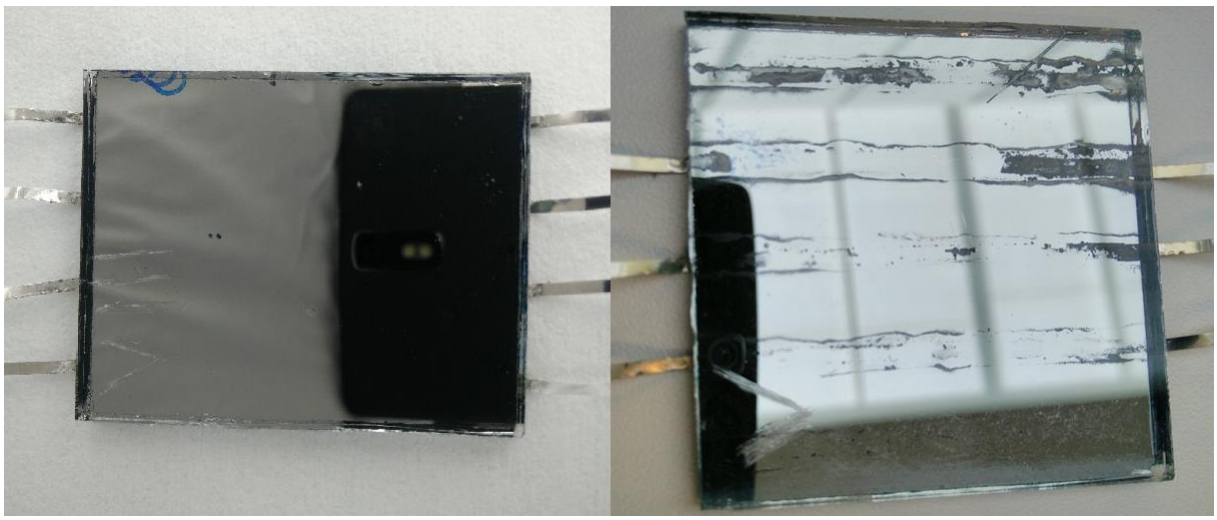

Figure 40: Backsides USS $MoSe_2$ samples before (left) and after (right) damp heat test

4.3 Electrically conductive tapes

The results from the ECT on both substrates were not usable to determine the contact resistance using the TLM method. The measured resistances were not always raising when increasing the distance between the ribbons. On molybdenum substrates the measured resistances varied between 1.5 and 8 Ω when using 3M 1181 tape and between 1.5 and 80 Ω with 3M T1245 tape. On $MoSe_2$ the measured resistances were even higher. The initial measured resistances varied between 200 and 15000 Ω with 3M 1181 tape and between 3 and 25 kΩ with 3M T1245 tape.

Despite not being able to determine the contact resistance, the samples were stressed. The 3M 1181 tape remained stuck on the substrates for both tests. On the other hand, 3 out of 25 3M T1245 ribbons came off due thermal cycling and 6 out of 25 ribbons due damp heat stressing.

Furthermore, the adhesives from both tapes affected the back contact layer when they were damp heat stressed. This is shown in Figure 41. Image A and B in Figure 41 are the backsides of $MoSe_2$ samples respectively with 3M 1181 and 3M T1245 tapes before stress testing. In image C and D, $MoSe_2$ samples with respectively 3M 1181 and 3M T1245 tapes are shown after the damp heat test. On some areas, the back contact layer is completely removed.

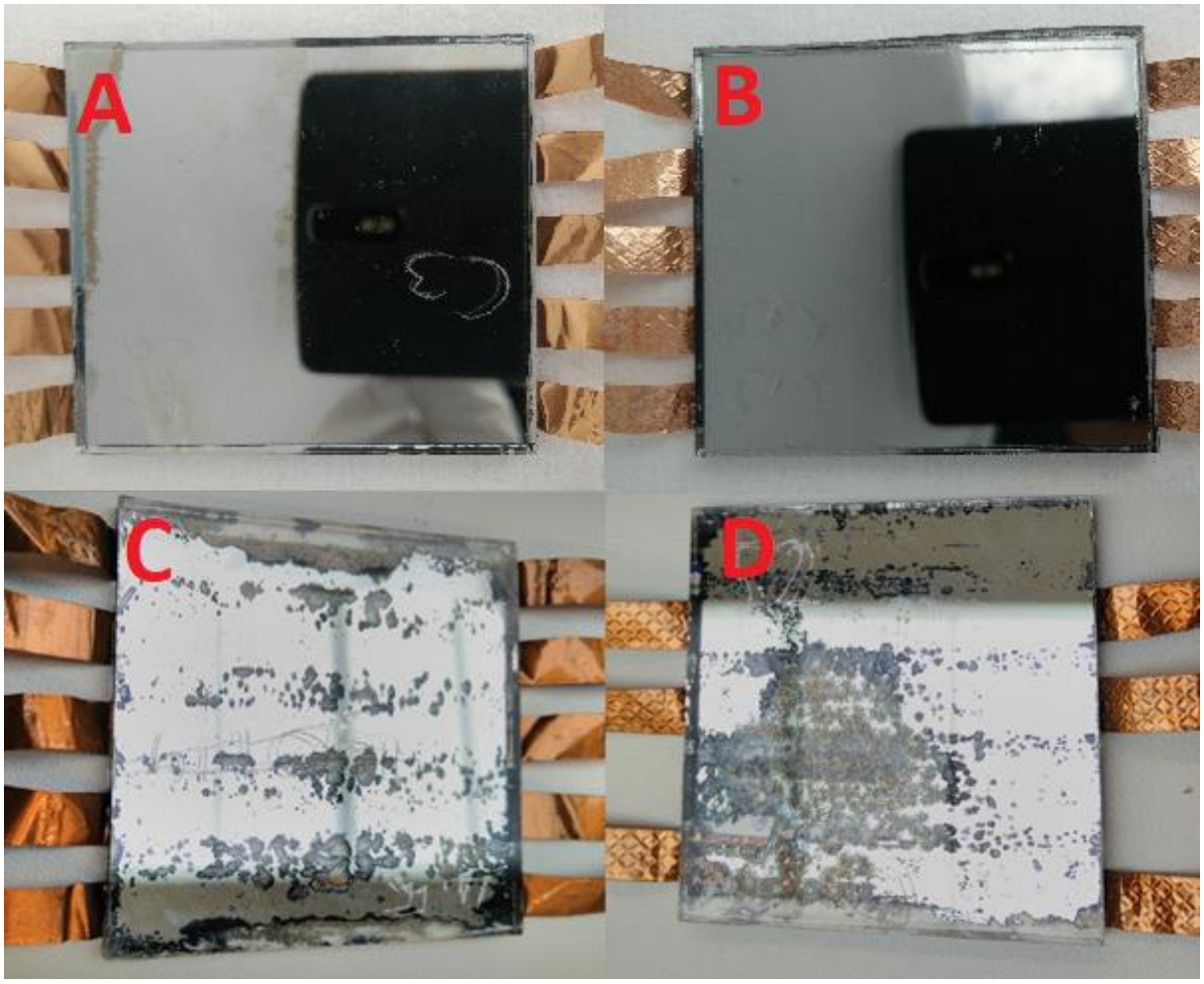

Figure 41: Backside $MoSe_2$ samples with ECT

4.4 Overview bonding methods

Directly comparing the contact resistances from the bonding techniques will not take the contact surface into account. To prevent this, a comparison is made between the contact resistivities of each bonding method.

The contact resistivity evolution of the USS and USW interconnections on $MoSe_2$ substrates is shown in Figure 42. The first 280 hours, the contact resistivity of both methods did not increase. Afterwards, the contact resistivity of the USS connections started to increase while the USW bonds remained constant for the first 450 hours.

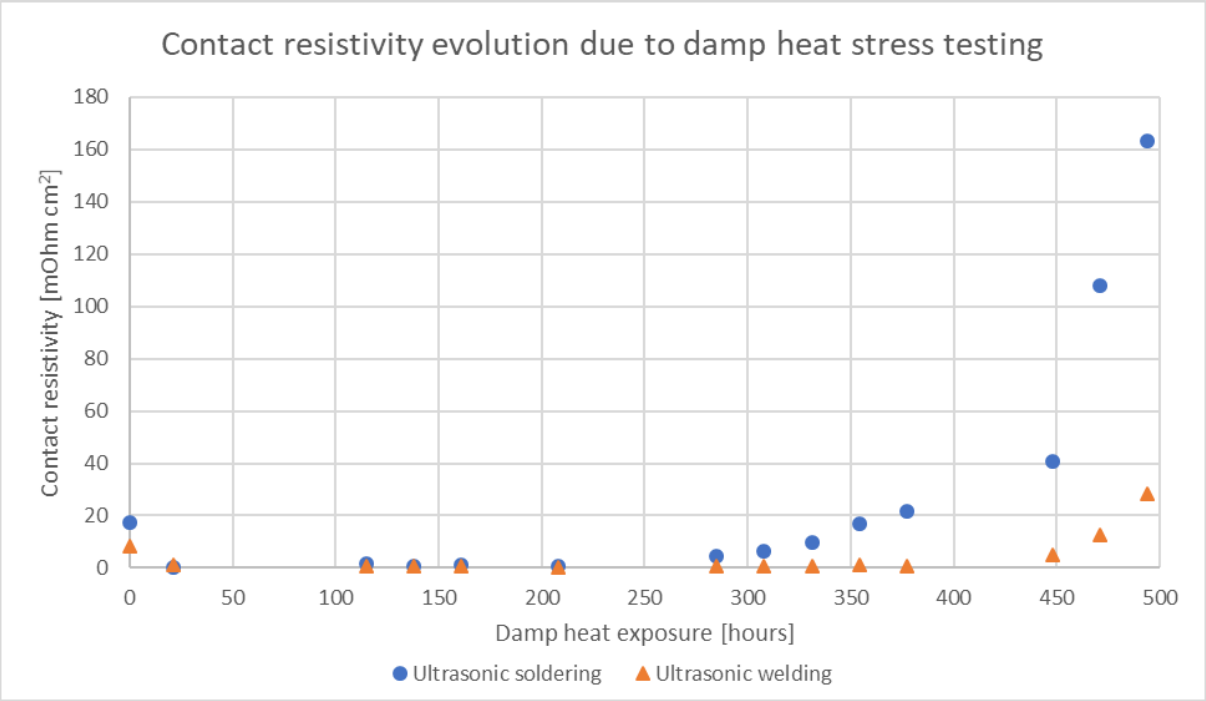

Figure 42: Contact resistivity evolution due to damp heat stress testing on $MoSe_2$ samples

The contact resistivities from the ECT are not included in this chart. The measured resistances were about 1000 times higher than the resistances from USS and USW. Besides, the measurements were not consistent enough to determine the contact resistance using the TLM method.

The stressing due to thermal cycling did not affect the bonds made with USS, USW and 3M 1181 tapes. On the other hand, the interconnections with the 3M T1245 tapes (first column of samples on the image) started detaching. After 92 cycles, three ribbons were completely detached from the sample. An optical overview is shown in Figure 43.

In contrast, there is more degradation on the damp heat stressed samples visible as shown in Figure 44. The adhesive from both ECT as well as the USS samples affected the substrate negatively. On the other hand, the USW samples did not have any visible degradation on the substrates. The only degradation detected by the USW bonds, was the increase of contact resistance due to damp heat.

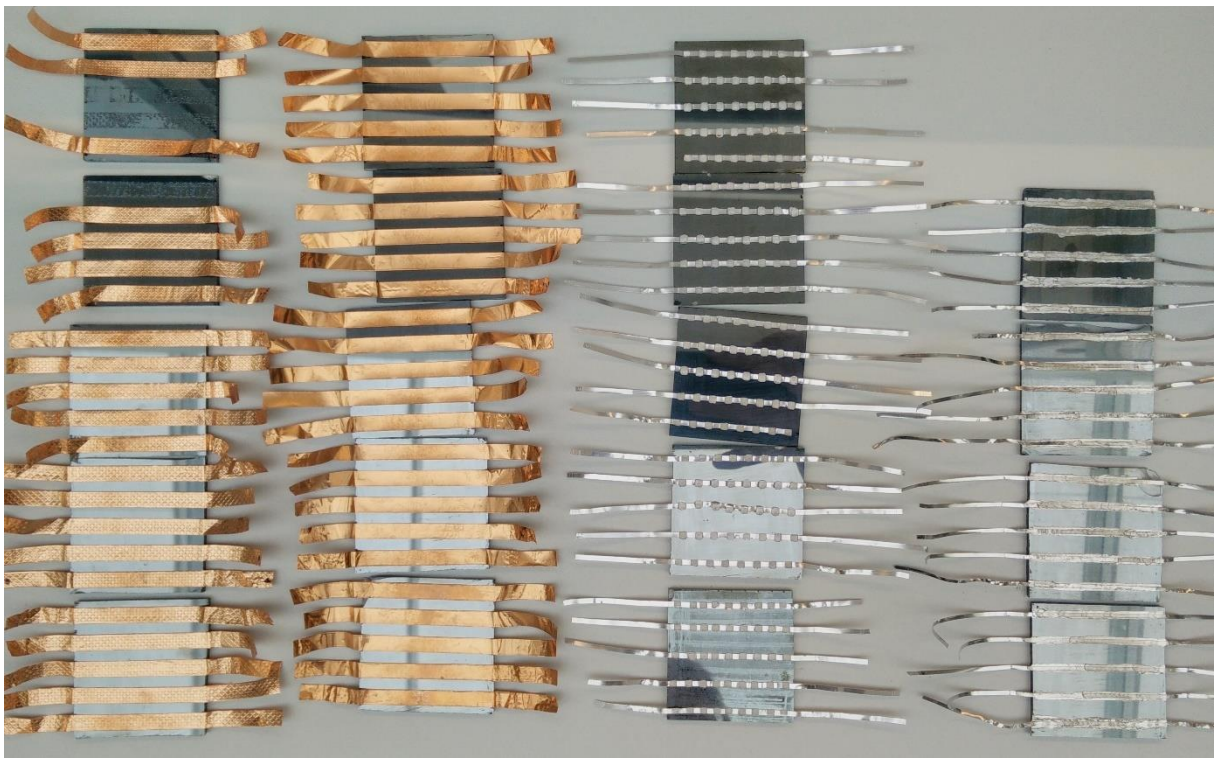

Figure 43: $MoSe_2$ sample overview after thermal cycling test

Figure 44: $MoSe_2$ sample overview after damp heat test

5 Conclusion

This master's thesis started with a literature review which is described in chapter 2, whereby three potential bonding methods, namely USS, USW and ECT, have been analysed. These methods are already being applied in other sectors. Furthermore, a study over specific test conditions specified by the IEC 61646 norm was studied. These tests methods are used to test the reliability of photovoltaic modules. Lastly, characterization methods were reviewed to measure the degradation. With this information a research method has been set up.

As described in chapter 3, the bonding techniques were applied on Mo as well as $MoSe_2$ substrates. After determining the initial contact resistances for all bonding methods and both substrates using TLM, a first comparison was made. The results indicated that the contact resistances on the $MoSe_2$ substrates were higher than on the Mo substrates. This extra $MoSe_2$ layer could also be seen on images made with the SEM. Besides, the contact resistances from the ECT were about 1000 times higher than the contact resistances from USS and USW.

Next, the $MoSe_2$ samples were stressed due to thermal cycling and damp heat. The results from the stress tests and the SEM images are presented in chapter 4. The samples which were stressed due to thermal cycling did not show any significant degradation after 92 cycles. On the other hand, degradation was visible on the damp heat stressed samples. Besides the degradation of the interconnections, degradation was also visible on the substrates from the USS and ECT samples. The contact resistivity increased the least at the USW samples due to damp heat stress. While running these tests, none of the USW ribbons was detached.

At the end of this master's thesis, it can be concluded that USW bonds have the best results to create connections on molybdenum back contacted CIGS TFPV. Further research is needed to find the cause of the $MoSe_2$ layer degradation on the substrates whereby the ECT and USS methods were used. A possible alternative for the ECT is the use of ECA to attach ribbons to the substrate. Lastly, an improvement that affects all methods would be the optimization of the removal of the CIGS layer and unwanted $MoSe_2$ layer.

References

[1] M. Theelen, *Degradation of CIGS solar cells*. Delft, 2015.

[2] Z. L. Ni and F. X. Ye, "Ultrasonic spot welding of aluminum alloys: A review," *J. Manuf. Process.*, vol. 35, pp. 580–594, Oct. 2018.

[3] J. Luo, Y. Zhao, M. Chen, and Y. Yao, "Electrically conductive adhesives based on thermoplastic polyurethane filled with carbon nanotubes," in *China Semiconductor Technology International Conference 2016, CSTIC 2016*, 2016.

[4] X. Yu, W. Xing, and M. Ding, "Ultrasonic semi-solid coating soldering 6061 aluminum alloys with Sn–Pb–Zn alloys," *Ultrason. Sonochem.*, vol. 31, pp. 216–221, Jul. 2016.

[5] H. Ji, M. Li, S. Ma, and M. Li, "Ni 3 Sn 4 -composed die bonded interface rapidly formed by ultrasonic-assisted soldering of Sn/Ni solder paste for high-temperature power device packaging," *Mater. Des.*, vol. 108, pp. 590–596, Oct. 2016.

[6] D. Abou-Ras, T. Kirchartz, and U. Rau, Eds., *Advanced Characterization Techniques for Thin Film Solar Cells*, 2nd ed. Weinheim, Germany: Wiley-VCH Verlag GmbH & Co. KGaA, 2016.

[7] S.-C. Chen *et al.*, "A Comprehensive Study of One-Step Selenization Process for Cu(In1−x Ga x)Se2 Thin Film Solar Cells," *Nanoscale Res. Lett.*, vol. 12, no. 1, p. 208, Dec. 2017.

[8] Z. Wu, J. Li, D. Timmer, K. Lozano, and S. Bose, "Study of processing variables on the electrical resistivity of conductive adhesives," *Int. J. Adhes. Adhes.*, vol. 29, no. 5, pp. 488–494, 2008.

[9] J. L. Harthoorn, *Ultrasonic metal welding*. Eindhoven: Technische Hogeschool Eindhoven, 1978.

[10] S. ichi Matsuoka and H. Imai, "Direct welding of different metals used ultrasonic vibration," *J. Mater. Process. Technol.*, vol. 209, no. 2, pp. 954–960, Jan. 2009.

[11] M. Shakil, N. H. Tariq, M. Ahmad, M. A. Choudhary, J. I. Akhter, and S. S. Babu, "Effect of ultrasonic welding parameters on microstructure and mechanical properties of dissimilar joints," *Mater. Des.*, vol. 55, pp. 263–273, Mar. 2014.

[12] P. Vianco, F. Hosking, and J. A. Rejent, "Ultrasonic Soldering for Structural and Electronic Applications," *Weld. J.*, vol. 75, no. November, pp. 343–355, 1996.

[13] K. Graff, "Macrosonics in industry: Ultrasonic soldering," *Ultrasonics*, vol. 15, no. 2, pp. 75–81, Mar. 1977.

[14] U-bonder, "How ultrasonic soldering works." [Online]. Available: http://www.u-bonder.com/how-ultrasonic-soldering-works/. [Accessed: 28-Nov-2018].

[15] T. Nagaoka, Y. Morisada, M. Fukusumi, and T. Takemoto, "Joint strength of aluminum ultrasonic soldered under liquidus temperature of Sn–Zn hypereutectic solder," *J. Mater. Process. Technol.*, vol. 209, no. 11, pp. 5054–5059, Jun. 2009.

[16] Y. Li and C. P. Wong, "Recent advances of conductive adhesives as a lead-free alternative in electronic packaging: Materials, processing, reliability and applications," *Mater. Sci. Eng. R Reports*, vol. 51, no. 1–3, pp. 1–35, Jan. 2006.

[17] H. Kesten, "Percolation?," 2006.

[18] R. Arndt and R. Puto, “Basic Understanding of IEC Standard Testing for PV Panels,” *Tüv Süd*, no. 978, 2013.

[19] G. K. Reeves and H. B. Harrison, “Obtaining the specific contact resistance from transmission line model measurements,” *IEEE Electron Device Lett.*, vol. 3, no. 5, pp. 111–113, May 1982.

[20] R. Janoch, A. M. Gabor, A. Anselmo, and C. E. Dube, “Contact resistance measurement - Observations on technique and test parameters,” *2015 IEEE 42nd Photovolt. Spec. Conf. PVSC 2015*, no. June, 2015.

[21] D. R. Moore, “An Introduction to the Special Issue on Peel Testing,” *Int. J. Adhes. Adhes.*, vol. 28, no. 4–5, pp. 153–157, Jun. 2008.

[22] Y. Su, M. de Rooij, W. Grouve, and L. Warnet, “Characterisation of metal–thermoplastic composite hybrid joints by means of a mandrel peel test,” *Compos. Part B Eng.*, vol. 95, pp. 293–300, Jun. 2016.

[23] D. J. Stokes, *Principles and Practice of Variable Pressure/Environmental Scanning Electron Microscopy (VP-ESEM)*. Chichester, UK: John Wiley & Sons, Ltd, 2008.